

**Integrating Remote Sensing, Behavior Modeling, and  
Machine Learning to Better Understand the Patterns and  
Drivers of Wildfire**

by

**A. L. DeCastro**

B.S., University of Colorado Boulder, 2017

M.S., University of Colorado Boulder, 2017

A thesis submitted to the  
Faculty of the Graduate School of the  
University of Colorado in partial fulfillment  
of the requirements for the degree of  
Doctor of Philosophy  
Department of Geography

2022

Committee Members:

Jennifer K. Balch, Chair

Katja Friedrich

Stefan Leyk

Colleen Reid

Christine Wiedinmyer

DeCastro, A. L. (Ph.D., Geography)

Integrating Remote Sensing, Behavior Modeling, and Machine Learning to Better Understand the  
Patterns and Drivers of Wildfire

Thesis directed by Prof. Jennifer K. Balch

Our understanding of and approach to fire is becoming increasingly important due to population increase and climate change. Current management strategies, which are focused mostly on basic resilience are not enough given the increasing wildland-urban interface and climate conditions ripe for wildfire. Informing future management strategies requires furthering our understanding of fire spread at a regional scale – the scale at which management decisions are made. The recent development of fire records cataloging thousands of fire events at daily and event-level resolutions has made it possible to investigate fire behavior at the regional scale. This research integrates remotely sensed data, wildland fire behavior modeling, and machine learning methods to further our understanding of the patterns and drivers of wildfire. High-resolution remotely-sensed datasets from several platforms were used to train random forest classification and regression models to identify drivers that matter at both the daily burned area and fire event scales, across individual case studies and collectively across thousands of events. WRF-Fire was used to investigate the intersection of drivers and how our current understanding of fire behavior, as represented by numeric models, compares to what we observe at sub-daily, daily, and event scales. Specifically it addresses data deficiencies in inhibiting the development of wildland fire behavior models, and identifies the most influential regional-scale drivers of daily fire growth. This work shows that environmental heterogeneity plays a critical role in daily fire spread; presents a method for updating fuel data for use within wildland fire behavior models; and bounds the uncertainty associated with inaccurate ignition data within burned area and propagation direction forecasts.

## Dedication

For Jane Goodall and Tony Hawk.

## Acknowledgements

Thank you Jennifer Balch for your encouragement and support throughout this adventure. Watching all that you have accomplished in the last few years, and how you've done it with warmth and compassion has been truly inspiring.

Thank you Michael Koontz for your camaraderie over the past few years, it has meant a lot to me. I really could not have done this without you. I look forward to the release of many fuzzy foster albatrosses with you in the future.

Thank you Jenny and JoAnna, Amy, Martha, and Rachel for validating this experience. At times when it could have been lonely, it wasn't, at times when it could have been crushing, it was funny. I have you to thank for that.

Thank you to my Research Applications Lab colleagues for supporting me and helping guide this work.

And thank you Bryce for holding down the fort, making spaghetti and birthday tacos, and enforcing outside time so that I could conquer this beast.

## Contents

### Chapter

<b>1</b>	Introduction	<b>1</b>
1.1	Background . . . . .	4
1.1.1	Wildfire Modeling . . . . .	4
1.1.2	Remote Sensing . . . . .	5
1.1.3	Machine Learning . . . . .	5
1.2	Research Overview . . . . .	6
<b>2</b>	<b>WRF-Fire Simulated Burned Area and Propagation Direction Sensitivity to Initiation Point</b>	
	Location and Time	<b>8</b>
2.1	Introduction . . . . .	8
2.2	Materials and Methods . . . . .	10
2.2.1	WRF-Fire . . . . .	10
2.2.2	Incident report analysis . . . . .	11
2.2.3	Case study selection . . . . .	12
2.3	Results . . . . .	15
2.3.1	Effects of initiation point location on forecast burn area . . . . .	17
2.3.2	Effects of initiation time on forecast area . . . . .	18
2.3.3	Effects of initiation point location on forecast propagation direction . . . . .	19
2.3.4	Effects of initiation time on forecast propagation direction . . . . .	20

2.3.5	Effects of both initiation point location and initiation time on forecast area and propagation direction . . . . .	21
2.4	Discussion . . . . .	22
2.5	Conclusions . . . . .	25
<b>3</b>	<b>A Computationally Efficient Method for Updating Fuel Inputs for Wildfire Behavior Models Using Sentinel Imagery and Random Forest Classification</b>	<b>27</b>
3.1	Introduction . . . . .	27
3.2	Materials and Methods . . . . .	29
3.2.1	The East Troublesome Fire Case Study . . . . .	29
3.2.2	Machine Learning Approach . . . . .	29
3.2.3	WRF-Fire . . . . .	32
3.3	Results . . . . .	36
3.4	Discussion . . . . .	41
3.5	Conclusion . . . . .	44
<b>4</b>	<b>Regional-Scale Drivers of Daily Fire Growth Across the Contiguous United States</b>	<b>45</b>
4.1	Introduction . . . . .	45
4.2	Methods . . . . .	47
4.2.1	Dataset . . . . .	47
4.2.2	Random Forest Regression Model . . . . .	49
4.3	Results . . . . .	51
4.3.1	Marine West Coast Forests . . . . .	51
4.3.2	Mediterranean California . . . . .	53
4.3.3	Tropical Wet Forests . . . . .	57
4.4	Discussion . . . . .	61
4.5	Conclusion . . . . .	64

<b>5</b>	<b>FIRED Linear Forward Rate of Spread; How fast are our fastest fires?</b>	<b>65</b>
5.1	Introduction . . . . .	65
5.2	Methods . . . . .	66
5.2.1	Bounding Fire Area and Calculating RoS Using Ellipses . . . . .	66
5.2.2	Determining Fires of Unusual Size . . . . .	74
<b>6</b>	<b>Conclusion</b>	<b>75</b>
6.1	Introduction . . . . .	75
6.2	Overall Findings . . . . .	75
6.3	Contributions . . . . .	76
6.3.1	Fire Forecasting . . . . .	76
6.3.2	Future Policy Development . . . . .	77
6.4	Future Work . . . . .	77
6.5	Closing Summary . . . . .	78
	<b>Bibliography</b>	<b>79</b>

## Tables

### Table

2.1	Ten 2018 Colorado wildland fire case study’s detection dates and times . . . . .	13
2.2	Generalized Linear Model Summary for Modeling the Range of Forecast Burn Area Values . . . . .	24
2.3	Generalized Linear Model Summary for Modeling the Range of Forecast Propagation Direction Values . . . . .	25
3.1	Random forest classifier confusion matrix . . . . .	36
3.2	Random forest classifier precision, recall, and F1-scores . . . . .	36
3.3	Summary of simulation and observed values . . . . .	40
4.1	Summary of the fire driver dataset . . . . .	50

## Figures

### Figure

2.1	Reported detection location for the Indian Valley Fire . . . . .	12
2.2	Ten 2018 Colorado wildland fire case studies . . . . .	13
2.3	Derived initiation points for case study simulations . . . . .	14
2.4	Distribution of simulated burned area and propagation direction by distance from detection location . . . . .	16
2.5	Distribution of simulated burned area and propagation direction by time of day . . .	17
2.6	Range of forecast burned areas for each case study . . . . .	18
2.7	Range of forecast burned areas for each initiation time . . . . .	19
2.8	Forecast direction of propagation by distance away from the detection location . . .	20
2.9	Forecast direction of propagation by initiation time . . . . .	21
2.10	Simulated burned areas for the 416 Fire case study . . . . .	22
3.1	Tree mortality classes mapped to Scott and Burgan fuel models . . . . .	32
3.2	WRF-Fire two-domain setup . . . . .	34
3.3	Unmodified and modified fuel layers used in WRF-Fire simulations . . . . .	35
3.4	Simulated fire progression compared with observations of the East Troublesome Fire for 10/22/20 0630 UTC . . . . .	38
3.5	Simulated fire progression compared with observations of the East Troublesome Fire for 10/23/2020 0230 UTC . . . . .	38

3.6	Time series of simulated and observed burned area . . . . .	39
3.7	Time series comparison of wind conditions from each simulation . . . . .	41
3.8	Permutation feature importance for fuel-adjustment random forest features . . . . .	43
4.1	EPA Level I ecoregions subset to CONUS with the FIRED daily burned area polygons	48
4.2	Marine West Coast Forest Daily Fire Growth Permutation Feature Importance . . .	52
4.3	Marine West Coast Forest EPA Level III Ecoregion and Daily Fire Growth Partial Dependence Plot . . . . .	53
4.4	Mediterranean California Daily Fire Growth Permutation Feature Importance . . . .	54
4.5	Mediterranean California Rumble Index and Daily Fire Growth Partial Dependence Plot . . . . .	55
4.6	Mediterranean California Peak Daily Fire Growth Permutation Feature Importance	56
4.7	Mediterranean California Rumble Index and Peak Daily Fire Growth Partial Depen- dence Plot . . . . .	57
4.8	Tropical Wet Forests Daily Fire Growth Permutation Feature Importance . . . . .	58
4.9	Tropical Wet Forests Rumble Index and Daily Fire Growth Partial Dependence Plot	59
4.10	Tropical Wet Forests Peak Daily Fire Growth Permutation Feature Importance . . . .	60
4.11	Tropical Wet Forests Rumble Index and Peak Daily Fire Growth Partial Dependence Plot . . . . .	61
5.1	Day 1 of the Rim Fire in California from the FIRED record. . . . .	67
5.2	Day 2 of the Rim Fire in California from the FIRED record. . . . .	68
5.3	Day 3 of the Rim Fire in California from the FIRED record. . . . .	69
5.4	Day 4 of the Rim Fire in California from the FIRED record. . . . .	70
5.5	Calculating linear rate of spread; first step using the Rim Fire as an example . . . .	71
5.6	Calculating linear rate of spread; second step using the Rim Fire as an example . . .	72
5.7	Calculating linear rate of spread; third step using the Rim Fire as an example . . . .	72

## Chapter 1

### Introduction

In many parts of the globe our world is burning. Ten of the largest fire years on record have happened since 2000 [7]. The reasons for this are complicated, though the convergence of climate change and human activity, particularly the increasing development of the wildland-urban interface (WUI), has played a significant role [88, 28, 113]. Climate change has shifted fuel characteristics by changing the suitability of the environment and the mechanisms that determine the rise and fall of species populations [14, 31]. For example, the deserts of the Western United States (U.S.) are likely to see a difference in the spread of invasive grasses due to (human-caused) climate change. Cold-intolerant grasses benefit from a longer freeze-free season (shorter winter). Warmer temperatures lengthen the fire season, and the earlier onset of fires bring conditions that exaggerate the fire-invasive feedback loop [14]. In tropical climates, climate-induced droughts decrease photosynthesis, increase tree mortality and autotrophic respiration (a large source of  $\text{CO}_2$ ), promoting wildfire by providing available fuel in a previously fuel-limited system [31]. Larger, more frequent fires in these forests results in more greenhouse gases being released in large quantities, magnifying climate change [29]. There is also a temporal correlation between human-caused and lightning-caused fires from year to year, suggesting that the total number of fires that propagate is largely dependent on the fuel and meteorological conditions. Those conditions are becoming more favorable for fire propagation with climate change [23].

The development of the WUI has contributed to disastrous fires [29], due in part to fire frequency and ignition probabilities being linked to human population and road density [95]. When

compared to historic fire regimes, human-related ignitions have more than tripled the length of the wildfire season. In the US this is especially true during the spring [23], a season with previously low fire frequency in most regions. Additionally, the number of human-caused ignitions is increasing. Cattau, Wessman, Mahood, and Balch (2020) [38] found that human-caused ignitions have shown a 9% proportional increase between 1992 and 2015.

Human-related ignitions have expanded the extent of wildfire by bringing ignitions into regions with higher fuel moisture and net primary productivity (NPP). In the U.S. we see this increase in fire occurrence in areas with historically low lightning strike density (Mediterranean California climate) and in areas of low lightning occurrence and dry fuels (Eastern Temperate Forest climate) [23]. Flammable landscapes with intermediate population densities in the western U.S. and southeastern Australia are particularly affected by extreme wildfire events. However, the more densely populated northern Mediterranean Basin with a similar climate is less prone. This difference is thought to be due to regional land use, which reduces available fuels [30]. In the U.S., indigenous and traditional fire management systems (similar to the effects seen in the Mediterranean Basin) have been replaced by operational, large-scale firefighting and fuel management practices. These practices have also played a role in increasing the number of fires [29], and have contributed to the risk of more severe wildfires [128, 92, 53].

The increase in wildfire frequency, severity, and size has motivated discussion on mitigation and prevention. Current management strategies, which are focused mostly on basic resilience are not enough given the increasing WUI and climate conditions ripe for wildfire [90]. Response to active fire is aided by wildfire propagation forecasts generated through operational-use wildfire rate of spread models. These models help anticipate when and where a wildfire is likely to propagate given a set of inputs describing weather, terrain, and fuel conditions. Significant effort has been made to develop accurate forecasting capabilities, however, wildfire behavior models continue to have uncertainties due to input data and changing fire regimes that lessen their utility. In a 2013 study of 47 different fire behavior models, the mean percent error of fire rate of spread fell between 20-310% [50]. A later study found that while mean errors have decreased overall for fire prediction

models, models for operational application have not shown significant improvement [51]. Persistent uncertainties still originate from input data sets, particularly wind speed, wind direction, fuel model assignment, and ignition location and timing data [26]. [PhD research questions 1 and 2] These challenges are coupled with recent extreme fire behavior and fires occurring in new regions due to the convergence of climate change and human activity. Extreme fire behavior, defined here as unsteady, erratic fire spread [138], is difficult to model due to rapidly changing input conditions. The advent of fires in new regions exaggerates the problem of uncertainties originating from input data. Fuel and ignition data are less available from areas not historically prone to fire. Subsequently, less is known about the interactions between the atmosphere, terrain, and fuels in these areas [36].

Increased remote sensing data and advancements in machine learning have aided our understanding of wildfire and its associated drivers. Specifically, improvements have been made in our ability to model wind over complex terrain [60, 109, 104], describe and map fuel moisture [131, 89], advance our understanding of the role of fuel scale in modeling [132], as well as the role of fuels in fire behavior [84]. However, we continue to have gaps in our understanding of fire behavior at the regional level -the level of operational management during active wildfire. [PhD research questions 3 and 4]

This work utilizes machine learning and remote sensing data to answer research questions concerning the uncertainties in wildfire behavior modeling due to input data and our understanding of wildfire behavior at a regional scale. Collectively, this work will contribute to our ability to respond to increasing wildfire frequency, severity, and size through wildfire forecast improvements and a deeper understanding of fire at the regional level. Specifically, the research questions are:

- (1) How does the use of wildfire detection time and location for behavior model initiation affect forecast burned area and propagation direction?
- (2) Can the fuel inputs used in wildfire behavior models adequately be updated through the use of remotely sensed data?
- (3) What are the most influential regional-scale drivers of fire growth across CONUS?
- (4) How fast, and where are the fastest fires across CONUS?

## 1.1 Background

### 1.1.1 Wildfire Modeling

Fons's Analysis of Fire Spread in Light Forest Fuels was published in 1946. It described the first in a long line of theoretical models working to describe wildfire behavior [106]. These theoretical models were generally sets of differential equations with boundary conditions reflecting the fuel temperature, air temperature, and wind speed, resulting in wildfire rate of spread as the solution. Despite being theoretical, they relied on observations for measures such as flame length and fuel diameter. Ultimately, the task of calculating inputs for theoretical models transitioned into the development of empirical and semi-empirical wildfire behavior models [130]. These models leaned more into the pragmatic space of providing accurate estimates of important measurements, such as rate of spread, rather than aiming to describe the underlying physical dynamics. As such, they were, and continue to be used in the realm of fire management.

One of the most prominent semi-empirical models was developed in the early 1970's [116]. Rothermel's set of rate of spread equations are based on a heat sink, heat source ratio that considers wind, terrain, and fuel characteristics. It allowed fire analysts to estimate fire rate of spread in the field by providing them with a worksheet and TI-59 calculator equipped with a program chip containing the set of equations. Rothermel's model is still widely used in the United States and Australia for operational-use wildfire behavior modeling, though now it is integrated into architecture that allows for more nuanced sets of inputs. Modeling systems such as FARSITE and WRF-Fire are implementations of Rothermel's rate of spread equations that incorporate data such as detailed weather forecasts and fine-scale elevation.

As mentioned previously, one of the main knowledge gaps for wildfire behavior modeling is a lack of data. In particular, fine-scale, sub-seasonal fuel data is needed, as well as accurate ignition location and timing information. The occurrence of fires in new regions exacerbates the issue of model uncertainties due to input data. Additionally, less is known about the interactions between the atmosphere, terrain, and fuels in areas not historically prone to wildfire [36].

### 1.1.2 Remote Sensing

At the start of wildfire modeling the observational inputs needed were gathered in situ or approximated. However, at the time Rothermel was developing the rate of spread equations so widely used today, the first of the Landsat satellites was being launched into orbit. Landsat 1 was designed for landmass observations. It's multispectral scanner (MSS) provided data from four spectral bands (visible green, visible red, and two near-infrared bands) at an 80 m ground resolution with an 18 day revisit time. While the revisit time was not frequent enough for observing wildfire for operational firefighting, it did provide information about fuels that could be used in wildfire behavior models. In fact, the family of Landsat satellites was instrumental in the development of the fuels data set LANDFIRE, which is commonly used in wildfire behavior models today. Specifically, imagery from Landsat 7 (2003 - 2012) provided vegetation indices for fuel mapping [120]. The modern iterations of LANDFIRE in use today still rely on those Landsat-derived indices.

One challenge associated with the use of LANDFIRE data sets is that they are updated at a rate outpaced by disturbance events. This has the effect of skewing wildfire behavior model results because the input data no longer reflects the fuel conditions present. Many research efforts have focused on estimating similar data to describe fuel, terrain, and meteorological conditions relevant to wildfire. These have included mapping fuel characteristics for fire management [76]; mapping wildfire burn severity, a metric of biological impact [78, 73]; spatio-temporal patterns of biophysical conditions [90]; canopy fuel characteristics [20]; and fuel moisture content [89, 110]. The key knowledge gap in understanding fuels is geospatial layers at fine enough temporal and spatial resolution that reflects the conditions that will promote or dampen fire [79, 77, 26].

### 1.1.3 Machine Learning

Machine learning models are appropriate for modeling complex interactions between systems, wildfire and its associated drivers included. Several of the aforementioned studies implemented machine learning to determine their findings. For example, McCandless, Kosović, and Petzke

(2020) [89] developed a random forest model trained on MODIS reflectance values and hydrology forecasts to estimate live and dead fuel moisture values daily across CONUS. Arellano-Pérez, Castedo-Dorado, López-Sánchez, González-Ferreiro, Yang, Díaz-Varela, and Ruiz-González (2018) [20] compared several machine learning models to determine the most accurate estimates of canopy fuel characteristics.

A main concern surrounding the use of machine learning is that the key interactions between variables are difficult to interpret (the ‘black box’ problem). This remains an issue, especially when compared to models traditionally used for inference.

## 1.2 Research Overview

A combination of remote sensing and machine learning approaches can improve fire behavior modeling efforts: better constraint of ignition point location and timing and higher temporal and spatial resolution of fuels. Research question (1) How does the use of wildfire detection time and location for behavior model initiation affect forecast burned area and propagation direction? focuses on the initiation point of WRF-Fire. Despite being infrequently considered, the accuracy of the initiation point is quite important. It determines the wind vector, terrain and fuel at the start of the model. Yet, models are consistently initiated from inaccurate location and time estimates. The sensitivity study described in Chapter 1 highlights the importance of obtaining accurate ignition data and shows that the range of values for burned area and propagation direction forecasts depends on the heterogeneity of the wind, terrain, and fuel inputs.

Research addressing question (2) Can the fuel inputs used in wildfire behavior models adequately be updated through the use of remotely sensed data? gives a flexible method of updating the LANDFIRE fuel layers. The fuel layers are gridded data sets where each cell contains a profile of fuel characteristics such as moisture of extinction and fuel bed depth. As such, wildfire behavior model architecture relies on those profiles as input. Chapter 2 outlines a method of transitioning from Sentinel imagery and aerial USGS tree mortality surveys to fuel inputs for use in WRF-Fire. A case study of Colorado’s 2020 East Troublesome Fire is used as an example. The fuel model data

(for use in wildland fire behavior modeling) available to incident commanders at the time of the fire had last been calculated in 2016, and represented healthy conifer forest and shrubland. Post-2016 the area of the fire experienced significant tree mortality due to beetle infestation. A random forest regression model is used to estimate and update the fuel model layer for the fire domain based on the satellite imagery and tree mortality surveys. While this example focuses on accurately representing dead, downed timber, though the method should translate to other conditions.

Scaling from our understanding of fire propagation at the individual event level through WRF-Fire to exploration of fire spread across thousands of events detected by remote sensing offers the opportunity to translate across scales. Research question (3) What are the most influential regional-scale drivers of fire growth across CONUS? makes use of the Fire Event Delineated (FIRED) data set to determine regional-scale wildfire drivers. The Rothermel rate of spread equations are applied indiscriminately to simulate wildfires across CONUS, yet we see an increase in empirical modeling at a regional-scale, aiming to estimate rate of spread using fuels, weather conditions, and terrain specific to individual regions. Are there drivers that are region-specific that should be considered more thoughtfully in behavior models? The drivers are determined by training a random forest model to estimate burned area based on remotely sensed data representing fuel, terrain, and meteorological characteristics. This work shows that environmental heterogeneity plays a key role in daily fire spread across CONUS.

Work concerning the last research question, question (4) How fast, and where are the fastest fires across CONUS? attaches a forward rate of spread metric to each of the FIRED daily burned areas. This metric is important to operational firefighting as well as our understanding of fire speed, as it gives a sense of how fast a fire is travelling. By calculating this metric for the FIRED record, we can determine where the fastest fires have been historically, which has not yet been done. While some work has been done to estimate growth, there is no systematic way that the linear rate of growth has yet been estimated across fire events in the satellite record. This step is critical to our ability to respond to the most dangerous fires.

## Chapter 2

### WRF-Fire Simulated Burned Area and Propagation Direction Sensitivity to Initiation Point Location and Time

#### 2.1 Introduction

How does the time and location of a wildfire detection point affect wildland fire behavior model forecasts? Wildland fire behavior models are often initiated using an estimated ignition point (referred to here as a ‘detection point’) with an unknown amount of uncertainty in its time and location. Actual ignitions (where and when the fire actually started) may never be known with absolute accuracy, and detection points are frequently used to initiate model simulations in their absence.

The primary purpose of a detection point, at least initially, is to aid firefighters in locating a fire after it has been detected. The detection is a best guess at where and when a fire started and may be adjusted in the fire report as the fire progresses and more information is gained. For example, the point of origin for the Ryan Fire in Colorado, 2018, was estimated at 39.06757 latitude, -105.1443 longitude. Later in the fire event, that location estimate was shifted to 39.05989 latitude, -105.1439 longitude (a difference of about 855 m). As the precise time of the ignition is rarely known with certainty, the time of detection is recorded in the fire report with an estimate of the fire’s size at the time of discovery. Along with the size estimate and time of discovery, the available fuels, topography, and atmospheric conditions help to give a sense of how long the fire has been burning. While this means that both the location and time of ignition are estimates with an unknown amount of uncertainty, they meet the needs of fire management. That is, the

detection does not have to accurately represent the ignition time and location for effective wildland fire response, it simply needs to give a sense of the proximity and size of the fire.

However, in the context of wildland fire behavior modeling, the use of a wildland fire detection will have implications for the initialization parameters of the model. The starting point and time determine the initial wind, fuel, and terrain conditions for the model simulation. Uncertainties in the detection translate to uncertainties in how representative the initialization parameters are of the actual conditions at the location and time of the ignition.

Wildland fire behavior models are used to further our understanding of fire behavior through experimentation and comparison with observation data [68]. These models are also used for operational management where fire forecasts aid in determining suppression strategies and the allocation of resources [103]. However, the uncertainty associated with wildland fire behavior model output can lead to diminished faith and use of fire forecasts [111].

Both contexts, wildland fire research and operational use, benefit from an improved understanding of wildland fire behavior model limitations, including those introduced through input data. Sensitivity studies have investigated wildland fire behavior model sensitivity to fuel characteristics [99, 21], the combination of meteorological conditions and fuels [41], and meteorological conditions [17]. Bachmann and Allgöwer's (2002) [22] study of uncertainty propagation within Rothermel's rate of spread equations comprehensively investigates 17 different input variables. Benali et al, (2017) [26] examined the uncertainty associated with fuels, winds, and ignition locations. However, to the best of our knowledge, the sensitivity of wildland fire behavior models to initiation location and time is yet to be fully explored. This research examines the range of burned area values and propagation directions resulting from different initiation point locations and times. We examined the forecasts for ten Colorado 2018 wildland fire case studies, each initiated from a set of 17 different point locations, and three different starting times. Our results show that the location of the initiation point is important to the simulation results, more so than the time of initiation. A brief investigation of the range of fuel, wind, and terrain inputs shows that the number of fuel models, wind speeds, wind directions, and terrain slopes and aspects are important predictors of the range

of forecast burned area and propagation direction values. These results align with studies that have shown that environmental heterogeneity and compounding uncertainty affects wildland fire behavior model forecasts [22, 26]. The methods of this study, including case study selection and model setup are given in the next section. A discussion of the results, conclusion and recommendations follow.

## 2.2 Materials and Methods

### 2.2.1 WRF-Fire

WRF-Fire [86, 87] integrates the Weather Research and Forecasting (WRF) model [124] with a wildland surface fire-behavior physics module [44]. WRF is a community model used to study and forecast land-atmosphere interactions at different scales. Coupled with the fire-behavior physics module that implements the Rothermel rate of spread equations [116], WRF-Fire forecasts fire-atmosphere interactions driven by topographic, fuels, and weather data. The chosen model physics and dynamics options follow the operational WRF-Fire modeling setup, the Colorado Fire Prediction System, which was developed by the National Center for Atmospheric Research (NCAR).

The simulations for this study are performed using version 4.0.1 of WRF-Fire [85]. The simulations are run in WRF’s large eddy simulation (LES) [93] configuration following Jimenez et al. (2018) [72], which allows for the fire to be initiated in a space in which the boundary layer turbulence is fully developed and generated through interactions with the land surface specific to the fire domain. The initial and boundary conditions are provided by High-Resolution Rapid Refresh (HRRR) [27] forecasts from the National Oceanic and Atmospheric Administration (NOAA) at 3 km resolution, downscaled to 1 km over 117 km by 117 km domain centered on the model initiation point. The extent of the model domain is approximately 13 km by 13 km, with two nested model domains at grid spacings of 111 m and 27.75 m. The aspect, elevation, and slope inputs come from the LANDFIRE topography products, a layer with 30 m spatial resolution [121, 114]. The fuel models are brought into WRF-Fire through LANDFIRE’s 40 Scott and Burgan Fire Behavior Fuel

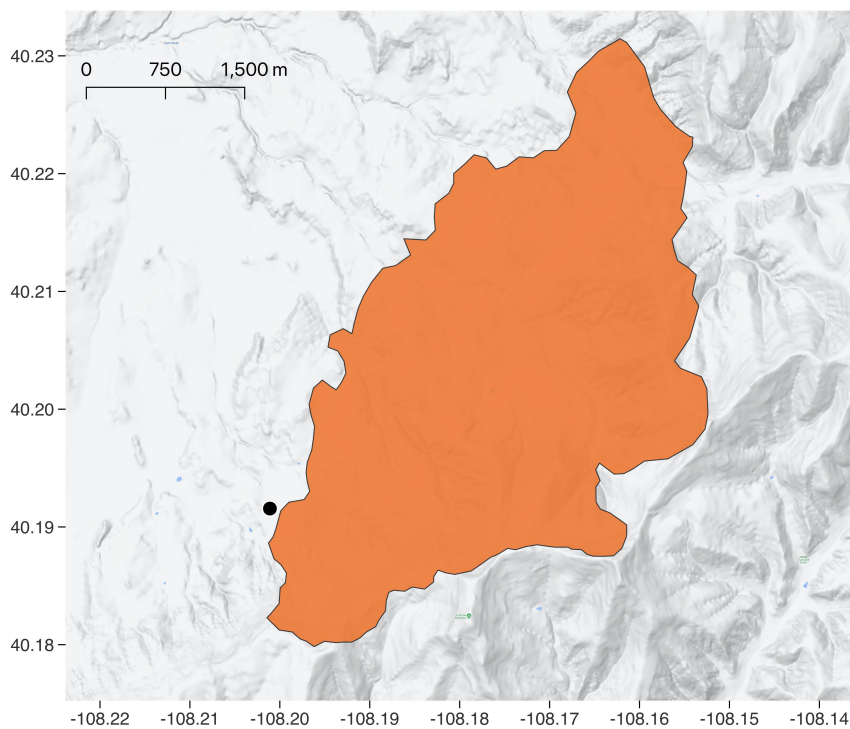
Models product, also at a 30 m spatial resolution [123].

### 2.2.2 Incident report analysis

Detection point information from fire reports was examined to help determine the structure of this sensitivity study. Integrated Reporting of Wildland-Fire Information (IRWIN) [6] hosts incident report information for 1705 fires in the state of Colorado for the year 2018. Out of the 1705, 1292 fires (75.8%) show a shift in the detection point location within the fire event's incident report. 27.9% of these fires had a detection point that shifted by less than 100 m, 25% had a detection point that shifted between 100 and 1000 m, and 47.1% had a detection point that shifted more than 1000 m. These shifts are representative of the uncertainty between the initial detection and the actual ignition location, and typically occur in the fire report days after the initial detection.

In addition to investigating the detection information in the incident reports, detection points were mapped alongside the first observed perimeter for fires with available data. This brief visual analysis shows that the detected location may be outside the first observed fire perimeters. Figure 2.1 shows an example using the Indian Valley Fire, which occurred in Colorado in 2018 and is used as a case study in this research. The detected point is approximately 135 m outside the closest location of the first observed burned area perimeter which was captured less than 5 hours after the fire was detected. We include this information simply to highlight the uncertainty in the reported wildland fire detections.

Figure 2.1: The first observed active fire perimeter (orange) for the Indian Valley Fire, Colorado 2018, and the fire's initial detection location (black dot).



### 2.2.3 Case study selection

Ten case studies of 2018 Colorado wildfires were selected from the National Fire Situational Awareness portal (National Interagency Fire Center) [7]. Out of the viable cases (cases with available detection data), an effort was made to choose case studies that spanned a variety of fuel and terrain characteristics, as well as a range of detection times. The search resulted in the cases mapped in Figure 2.2 and described in Table 2.1.

Figure 2.2: Ten Colorado wildland fire case studies from 2018, with initial detection locations (black dots).

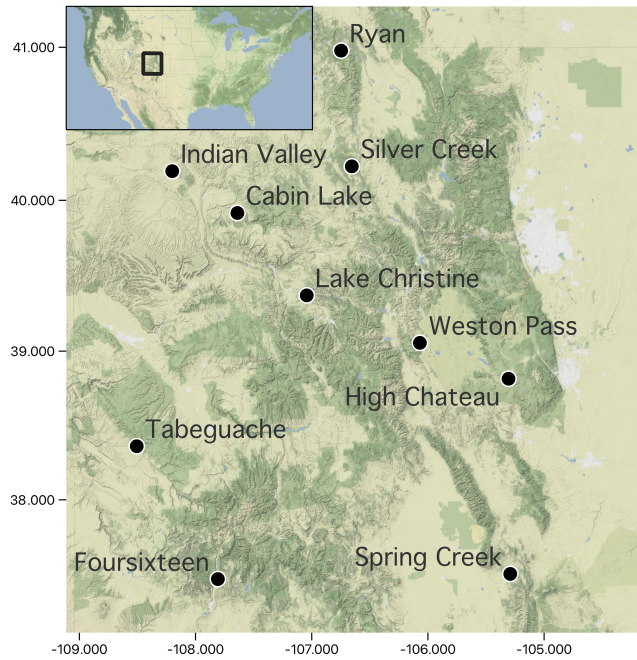


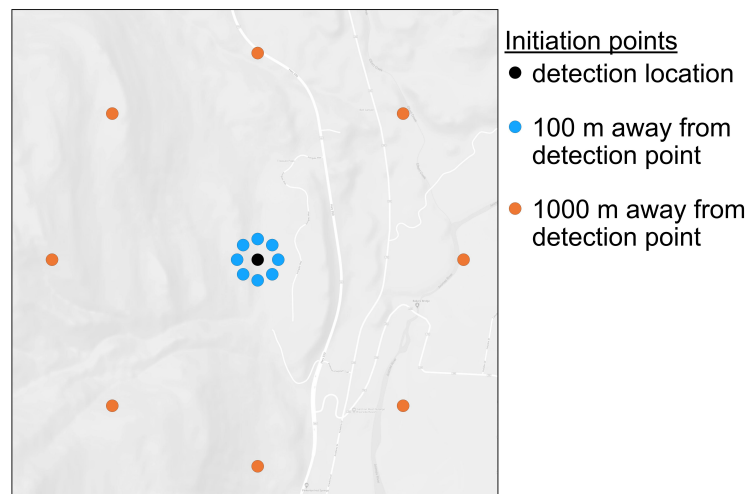
Table 2.1: Case study fire names, detection dates, and detection times (UTC).

Fire Name	Detection Date	Detection Time
416	2018-06-01	1602
Cabin Lake	2018-07-29	2000
High Chateau	2018-07-29	2000
Indian Valley	2018-07-20	2030
Lake Christine	2018-07-03	0011
Ryan	2018-09-16	0136
Silver Creek	2018-07-19	2030
Spring Creek	2018-06-27	2130
Tabeguache	2018-07-07	0434
Weston Pass	2018-06-28	2030

For each of the case studies, a set of model initiation points was derived from the reported

detection point. Eight points were selected in each of the cardinal and intercardinal directions 100 m away from the detection location, and likewise, eight more points were selected 1000 m away from the detection location as shown in Figure 2.3. The decision to calculate points 100 m and 1000 m away was determined through examination of the detection points recorded for 2018 Colorado wildfires, as described above. This covers the range of more than half of the shifts in detection location observed in the IRWIN record of 2018 Colorado fires.

Figure 2.3: Configuration of derived initiation points, shown for the 416 Fire case study. The reported detection point is shown in black, derived points 100 m away are shown in blue, and 1000 m away are shown in orange.



In total, each case study has 17 initiation points for simulation; the detection point, along with the 16 derived points. WRF-Fire simulations were run for each of the case studies, at each of these 17 points starting from the time of detection. This isolated the changed variable in the model setup to the initiation point location, providing model output from each case study's set of simulations to determine the effects of shifting the initiation location on forecast burned area and propagation direction. Simulations were also run from each of the 17 points at plus and minus six

hours from the detection time for each case study. For example, simulations of the 416 Fire were initiated at 1602 UTC (its detection time), as well as 1002 UTC and 2202 UTC. Simulating the case studies at these offset times provides data showing how the timing affects the modeled fire area and propagation direction.

Half of the case studies were detected in the early afternoon (1400 - 1530 MDT), with the remaining case studies detected either in the evening, late at night, or late morning. Starting simulations plus and minus six hours from these detection times provides a broad range of times to examine. The combined effects of shifts in both location and time are observed in the model output from simulations started at the shifted detection points and the augmented times. Cumulatively, each case study had 52 resulting forecasts to examine; one set of model output at each of the 17 locations and each of the three initiation times.

WRF-Fire provides model output at a user-defined time window. Model forecasts for this research are generated at an hourly time resolution. Specifically, the resulting model output from a six hour lead time (forecast fire area and direction of propagation from the sixth simulated hour) was examined. A six hour lead time, along with the total number of case studies, initiation time offsets, and initiation points, was chosen for two reasons; to keep within reasonable computational limits, and to generate output data with enough difference for comparison. For the sixth hour of each forecast, we calculated the forecast fire area as well as the direction of propagation. The direction of propagation is calculated using the direction of the vector from the initiation point to the centroid of the predicted fire area.

## 2.3 Results

Figure 2.4 and Figure 2.5 summarize the overall results of this research. The range of simulated burned areas and propagation direction remains more compact for simulations initiated 100 m away from the detection point than for simulations initiated 1000 m away from the detection point. However, no significant pattern is evident connecting the overall range of simulated fire areas and propagation directions to the time of day.

Figure 2.4: Distribution of the range of values for the simulated burned area and propagation directions by distance from the detection point. Each point represents the the values for a set of model results initiated from the points 100 m away from the detection point (orange) or 1000 m away from the detection point (blue) at the detection time, six hours before, or six hours after.

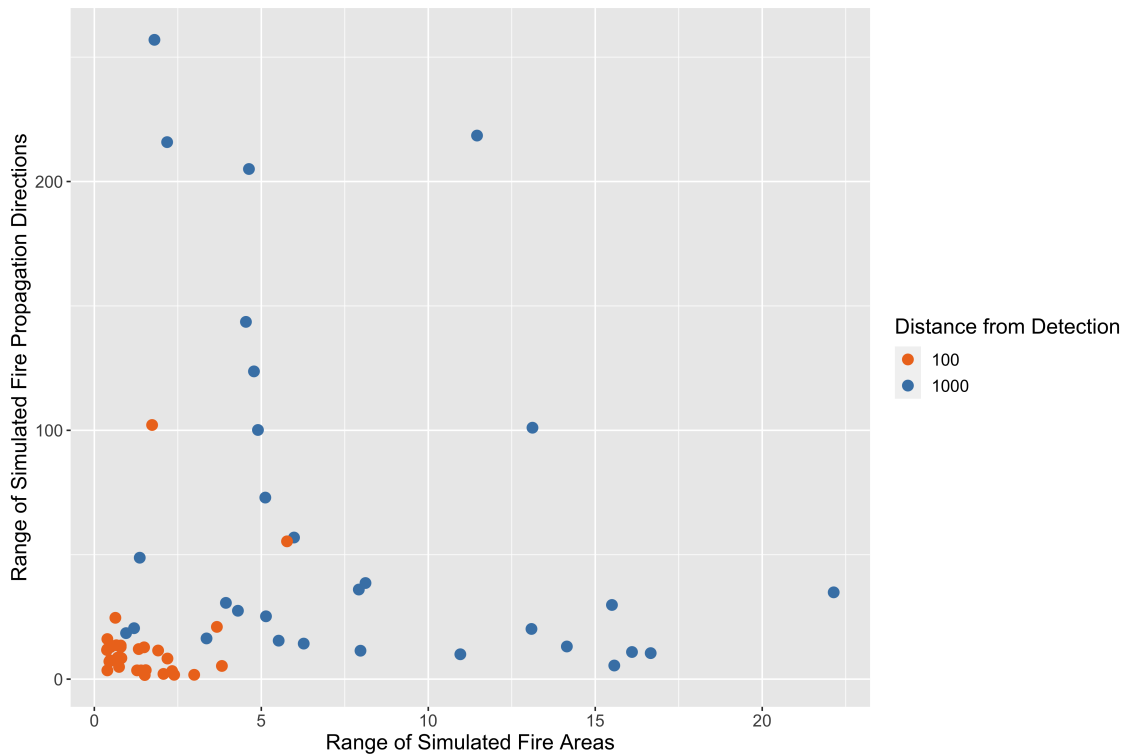


Figure 2.5: Distribution of the range of values for the simulated burned area and propagation directions by time of day. Each Time class represents four hours; "early": 2:00 a.m.-5:59 a.m., "morn": 6:00 a.m.-9:59 a.m., "mid": 10:00 a.m.-1:59 p.m., "aft": 2:00 p.m.-5:59 p.m., "eve": 6:00 p.m.-9:59 p.m., "night": 10:00 p.m.-1:59 a.m..

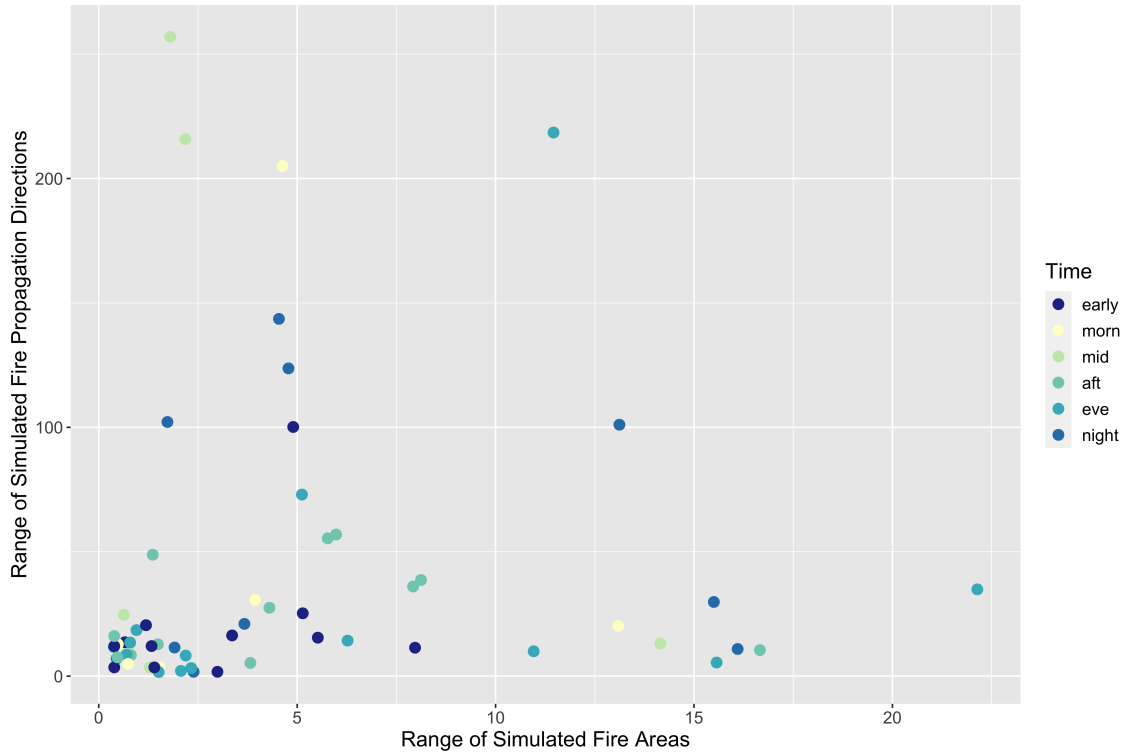
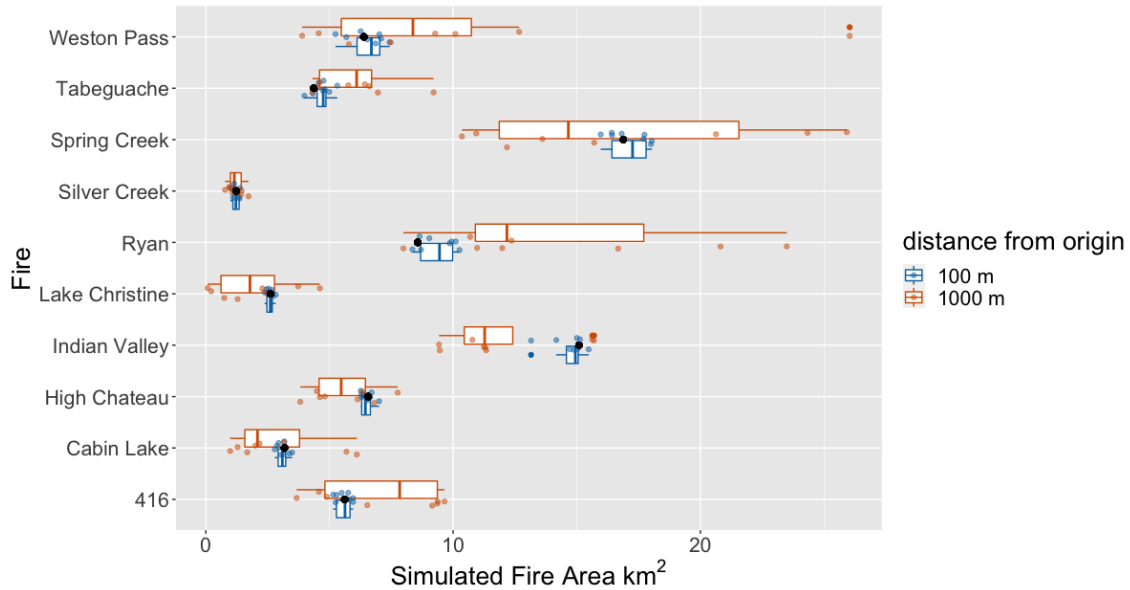


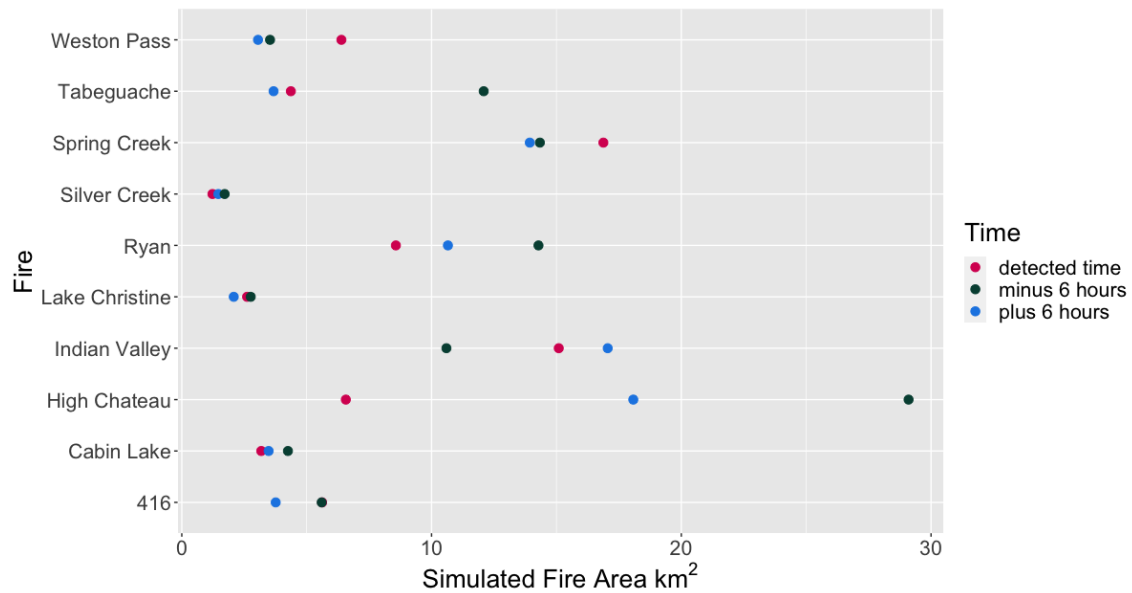
Figure 2.6: Forecast areas for each case study resulting from simulations initiated at the detection time and all 17 initiation points. Simulations initiated 1000 m away from the detection location had a broader range of forecast burn area values than simulations initiated 100 m away from the detection location.



### 2.3.2 Effects of initiation time on forecast area

The effect of shifting the simulation initiation time by six hours on the forecast area varies by case study. Considering simulations started from just the detected locations, the smallest range of forecast area values was (1.23 km<sup>2</sup> - 1.72 km<sup>2</sup>) from the Silver Creek Fire case study, and the largest was (6.57 km<sup>2</sup> - 29.10 km<sup>2</sup>) from the High Chateau Fire case study. Forecast fire area values simulated from the detected location at the detected time, plus and minus six hours for each case study are summarized in Figure 2.7 below.

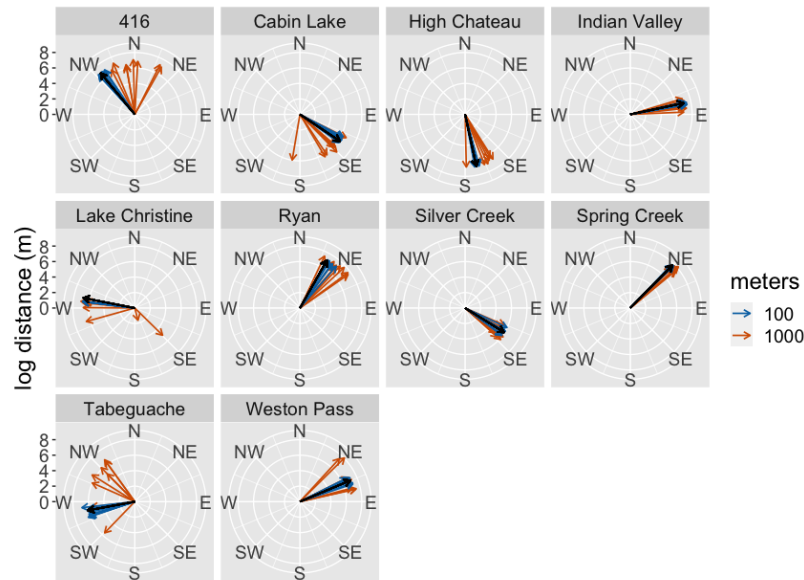
Figure 2.7: Forecast burned area at each case study's detection location initiated at the detection time (magenta), six hours before (dark green) and six hours after (blue). The range of forecast areas differs by case study.



### 2.3.3 Effects of initiation point location on forecast propagation direction

Figure 2.8 summarizes the forecast direction of propagation from case studies initiated at their respective detection times. Again, the range of values has a tendency to broaden with distance away from the detected fire location. Simulations of the Silver Creek Fire had the smallest range of values ( $113.51^\circ - 132.00^\circ$ ), while simulations of the 416 Fire had the largest ( $317.48^\circ - 29.27^\circ$ ).

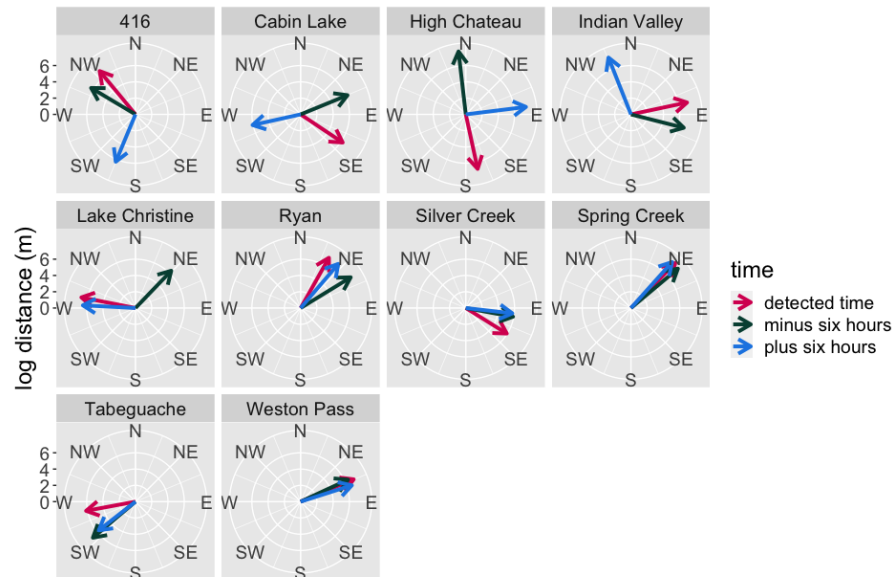
Figure 2.8: Forecast direction of propagation for case studies initiated at the time of detection. The range of propagation directions tends to be wider for simulations initiated 1000 m away (orange vectors) from the detection location than for those initiated 100 m away (blue vectors) from the detection location. The direction of the simulation initiated from the detection location is shown in black.



### 2.3.4 Effects of initiation time on forecast propagation direction

Forecast propagation direction simulated from the detected location at the detected time, plus and minus six hours for each case study are summarized in Figure 2.9. Again, the effects vary by case study. Considering simulations started from just the detected locations, the smallest range of forecast fire propagation directions was ( $67.24^\circ - 72.34^\circ$ ) from the Weston Pass Fire case study, and the largest was ( $67.77^\circ - 257.54^\circ$ ) from the Cabin Lake Fire case study.

Figure 2.9: Forecast propagation direction for simulations initiated at the detection location at the time of detection (magenta), six hours before (dark green), and six hours after (blue).

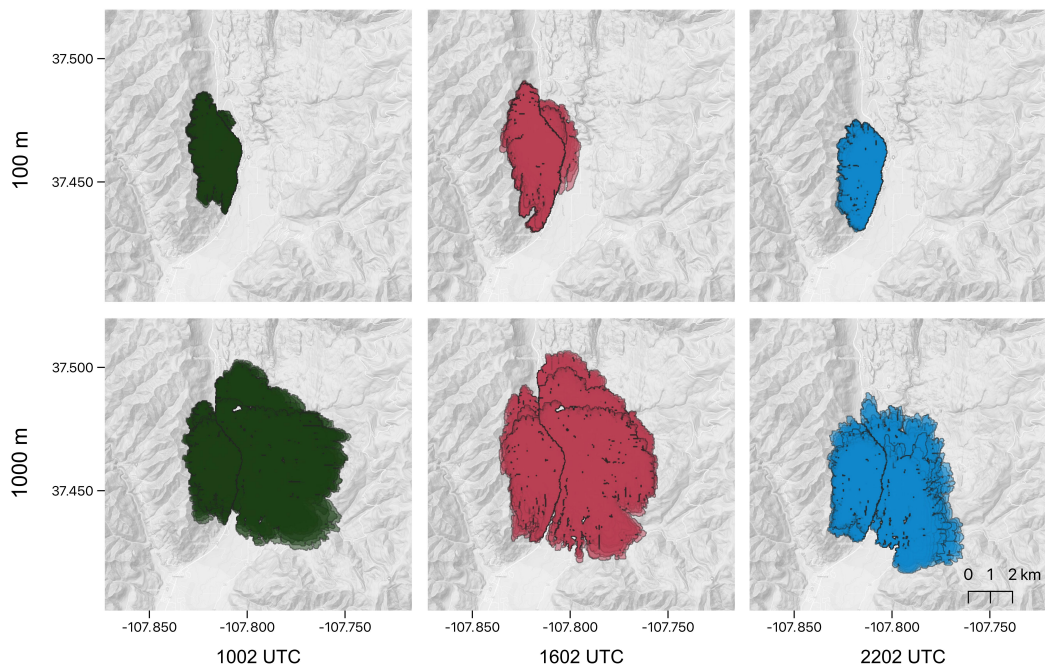


### 2.3.5 Effects of both initiation point location and initiation time on forecast area and propagation direction

Simulations of the 416 Fire are used for a closer look at the combined effects of initiation point location and time on simulated fire area and propagation direction. The results of this case study are summarized in Figure 2.10. The range of propagation directions is narrowest at the time of detection (10:02 a.m. MDT, 1602 UTC, a range of  $71.79^\circ$ ), while the range of propagation directions is wider both six hours before (4:02 a.m. MDT, 1002 UTC,  $213.70^\circ$ ) and six hours after the detection time (4:02 p.m. MDT, 2202 UTC,  $162.91^\circ$ ). The range of simulated burned areas resulting from initiation locations 100 meters away from the detected location are more compact than those resulting from initiation locations 1000 meters away from the detected location. The area difference for simulations 100 meters away from the detected location at the time of detection is  $0.81 \text{ km}^2$ , and  $5.98 \text{ km}^2$  for simulations 1000 meters away from the detected location. The area differences for simulations initiated six hours before the detection time are  $0.79 \text{ km}^2$  and  $1.78 \text{ km}^2$  for initiation points 100 meters and 1000 meters from the detection location, respectively. The area

differences for simulations initiated six hours after the detection time are  $1.73 \text{ km}^2$  and  $4.78 \text{ km}^2$  for initiation points 100 meters and 1000 meters from the detection location, respectively.

Figure 2.10: Forecast burned area perimeters for the 416 Fire case study. Simulations initiated at the detection location at the time of detection (magenta, center), six hours before (dark green, left), and six hours after (blue, right) at initiation points 100 m away from the detection points (top) and 1000 m away from the detection point (bottom).



## 2.4 Discussion

As shown, the range of forecast burned area and propagation direction values is strongly affected by the location of the initiation location, less so, if at all by the time of day. The Rothermel rate of spread equations implemented in WRF-Fire rely on several input values. Among these, the initiation location and time determine the fuel model (a set of fuel characteristics including load depth and fuel type), the wind vectors, and the terrain characteristics. For each domain of the fire case studies used in this research, the fuel model, 10 m height wind direction, 10 m height

wind speed, terrain aspect, and terrain slope were collected. The range of values for each of these variables was calculated for each simulation and used to fit a separate generalized linear model for each output variable (forecast burned area and propagation direction). Generalized linear models are used here to estimate the relationship between variables. Summaries for the models are shown in Table 2.2 and Table 2.3. The range of fuel models, wind directions and speeds, and aspects are important predictors of the range of forecast burned area values. The same is true of the range of forecast propagation directions, though the range of slope values is also important in this case. Essentially, this brief investigation shows that the range of forecast burned area and propagation direction values is related to the heterogeneity of the fire domain. In a space with consistent fuel models, slopes and aspects, with little variability in the wind speeds and wind directions across space and time, forecasts initiated at different locations and different times will result in similar burned areas and propagation directions. In a space with several different fuel models and more complex terrain, with variability in the wind speeds and wind directions across space and time, forecasts initiated at different locations and different times will result in wider ranges of burned area and propagation direction values.

Table 2.2: Generalized Linear Model Summary for Modeling the Range of Forecast Burn Area Values (area\_range) from the Range of Fuel Models (n\_fuel), Terrain Slope (slope\_range), Aspect (aspect\_range), 10 m Height Wind Direction (wdir\_range), and 10 m Height Wind Speed (wspd\_range). P-values and coefficients (in parentheses) are shown for each variable and the model's constant term.

<i>Dependent variable:</i>	
area_range	
n_fuel	-0.351*** (0.079)
slope_range	0.001 (0.009)
aspect_range	0.005*** (0.001)
wdir_range	0.010*** (0.004)
wspd_range	0.119* (0.065)
Constant	1.530*** (0.267)

*Note:* \*p<0.1; \*\*p<0.05; \*\*\*p<0.01

Table 2.3: Generalized Linear Model Summary for Modeling the Range of Forecast Propagation Direction Values (*dir\_range*) from the Range of Fuel Models (*n\_fuel*), Terrain Slope (*slope\_range*), Aspect (*aspect\_range*), 10 m Height Wind Direction (*wdir\_range*), and 10 m Height Wind Speed (*wspd\_range*). P-values and coefficients (in parentheses) are shown for each variable and the model's constant term.

<i>Dependent variable:</i>	
	<i>dir_range</i>
<i>n_fuel</i>	0.112*** (0.027)
<i>slope_range</i>	0.057*** (0.003)
<i>aspect_range</i>	0.002*** (0.0003)
<i>wdir_range</i>	0.017*** (0.001)
<i>wspd_range</i>	0.085*** (0.023)
Constant	1.395*** (0.126)

*Note:* \*p<0.1; \*\*p<0.05; \*\*\*p<0.01

While there are other possible sources of uncertainty in wildland fire behavior model inputs, this study shows the importance of using the best available ignition time and location data. For implementing wildland fire behavior models in the context of operational fire management, the detection information and any in-situ observations may be the best available at the time. In the context of wildland fire research, bounding the ignition information using remotely sensed data, as done in the work by Benali et al. (2017) [26] will aid in improving the model setup. The ability to do so will likely improve in the near future as higher-frequency, higher-resolution remotely sensed data becomes available. This advancement in technology will certainly inform wildland fire research, and has the potential to help provide near real-time active fire data, including ignition information.

## 2.5 Conclusions

As shown, the range of forecast burned area and propagation direction values is strongly affected by the location of the initiation location, and to a lesser degree by the time of initiation.

This is due to the input data associated with the initiation location and time. The location determines the fuel model and terrain characteristics, while both the time and location determine the wind conditions. Incident commanders and wildland fire researchers using wildland fire behavior models can anticipate that the range of forecast burned areas and propagation directions will be wider in heterogeneous fire domains, and more compact in homogeneous spaces.

## Chapter 3

### A Computationally Efficient Method for Updating Fuel Inputs for Wildfire Behavior Models Using Sentinel Imagery and Random Forest Classification

#### 3.1 Introduction

The coniferous forests of the lower Rocky Mountains are innately disposed to wildfire [71]. Trends toward a warmer, drier climate and rapid development of the wildland-urban interface (WUI) have increased wildfire risk to human life and property in this region [108]. Additionally, fuel accumulation through historic fire suppression and the rise in fuel aridity have contributed to the risk of more severe wildfires [34]. Wildfire frequency and severity are increasing in the Western United States [105], and the largest, most severe fires have occurred since 2004 [4], motivating national discussions on risk mitigation [10].

Wildfire behavior models may be used effectively to forecast fire area, propagation direction, and other metrics essential to operational firefighting, fuel treatment and our overall understanding of wildfire [36]. Fuel characteristics including fuel load depth, percent moisture of extinction, vegetation type, particle size, and heat content are important inputs for these models. Quantifying fuel characteristics in an accurate and timely way has been one of the main challenges of wildfire mitigation and operational management [77]. These models rely on accurate fuel data, and when data are available, the behavior models may be used reliably in pre-wildfire mitigation, and in active-fire suppression and management. However, wildfire fuels are dynamic on multiple time scales, from their response to hourly atmospheric conditions to their response to multi-year disturbance events such as drought or insect outbreaks. The publication of the fuel inputs commonly used for wildfire

behavior modeling may occur at a frequency outpaced by these disturbance events. However, these datasets provide a robust foundation that may be mindfully adjusted to provide wildfire behavior models with updated fuel information.

LANDFIRE [114], a program that develops and publishes national geo-spatial datasets, hosts a suite of wildfire fuel datasets used by fire scientists and forest management teams to suppress active wildfire and plan mitigation strategies. The LANDFIRE datasets include the Scott and Burgan 40 fuel models [123], which are commonly used in wildfire behavior modeling. The fuel models are profiles of fuel characteristics including fuel bed depth, fuel load, fuel moisture of extinction, vegetation composition, and surface-area-to-volume ratio. Most fuel data sets are created by mapping (or ‘crosswalking’ in fuel modeling terminology) remotely sensed data, such as satellite reflectance values, to fuel characteristics used in wildfire behavior models. To determine the appropriate fuel model for each location in a 30 m x 30 m grid across the contiguous United States (CONUS), the fuel data integrate remote sensing data, system ecology, gradient modeling, and landscape simulation. Composing fuel data sets is time consuming, and requires significant planning, resources, and funding. Understandably, the data sets are infrequently updated, which can be problematic when used as input for wildfire behavior modeling, particularly when used for operational wildfire management.

Here we present a method of refreshing fuel layer data using a case study of 2020 East Troublesome Fire in Colorado. While the most current LANDFIRE data available at the time of the fire showed the domain as healthy timber, shrub, and grassland, fire records show that the East Troublesome Fire burned through significant amounts of dead and downed timber. While this case study requires adjusting the fuel data to reflect beetle infestation and blowdown due to wind events, the same method could be applied to other scenarios such as representing fuels before recursive burning or a shift in vegetation type. The overall goals of this work are to estimate tree mortality severity using a random forest (RF) model trained on C-band Synthetic Aperture Radar (C-SAR) Sentinel-1 data, raw bands and vegetation indices from Sentinel-2 data, land cover vegetation classes from the United States Forest Service (USFS) Landscape Change Monitoring

System (LCMS), and the Insect and Disease Detection Surveys (IDS) from the US Forest Service; simulate a case study of the East Troublesome Fire using both the generated fuel data and the LANDFIRE data available at the time of the fire; and to compare the simulations' results with observed active fire data.

## **3.2 Materials and Methods**

### **3.2.1 The East Troublesome Fire Case Study**

The East Troublesome Fire was detected on October 14, 2020 northeast of Kremmling, Colorado in the Arapaho and Roosevelt National Forests. With low humidity recovery overnight and high winds, the area was perfectly primed for fast wildfire conditions. Within the first three days, the fire spread to approximately 10,000 acres. Within nine days, it had covered nearly 200,000 acres and crossed to the east side of the Continental Divide [5].

The East Troublesome Fire is an especially notable case study because it spread upwards of 87,000 acres in one 24-hour period (October 21 – 22, 2020). At the time of the fire, the available LANDFIRE fuel data set reflected fuel conditions from 2016. In 2016, much of the fire's domain was classified as standing healthy timber and shrub. However, between 2016 and 2020, the timber in the fire domain experienced pine beetle outbreak, drought, and wind storms resulting in fuel conditions described as jackstraw; a tumble of very dry, downed and standing trees [5]. Thus, we expect that a simulation of the East Troublesome Fire using the Scott and Burgan 40 fuel model layer available at the time of the fire would underestimate the burned area, as much of the fire domain was represented as healthy, standing timber and shrub in the dataset.

### **3.2.2 Machine Learning Approach**

To update the existing fuel layer for the East Troublesome case study, we trained a RF classifier to estimate severity of tree mortality based on Sentinel-1 and Sentinel-2 imagery [1, 2], the USFS-LCMS [3] and the USFS Insect and Disease Detection Survey (IDS) conducted in July

2019 [11]. These data were chosen to capture the greenness, texture, vegetation type, and level of tree mortality throughout the fire domain.

The Sentinel-1 system consists of two satellites, both in the same orbital plane, carrying C-SAR instrumentation. This research utilizes data collected in the instruments' interferometric wide swath (IW) mode, the main operational mode over land. The system has a revisit time of 5-7 days over the East Troublesome fire location, with a 10 m spatial resolution. C-SAR data is used effectively for land cover change and classification [8]. In this research, C-SAR data is included in the set of model inputs to provide information on surface texture; to help distinguish between features such as shrubs, standing timber, and downed timber.

The Sentinel-2 system also consists of two satellites, each carrying a multispectral instrument (MSI) that sample 13 spectral bands at spatial resolutions between 10-60 meters. The system has a revisit time over the case study location of approximately 5 days. Due to its relatively fine spatial and temporal resolution, data from this system has been used for land and maritime monitoring, as well as natural disaster management [9]. MSI data from Sentinel-2 is included to provide the RF with information on vegetation health, and to help distinguish between surface features.

The USFS-LCMS data set contains land cover change, land cover, and land use data at an annual resolution. These data are calculated by ensemble modeling techniques, using Landsat and Sentinel-2 imagery, terrain data, and LandTrendr and CCDC change detection algorithm results as inputs. The USFS-LCMS Land Cover product was used in this research to provide the model with a distinction between vegetation classes.

IDSs are conducted annually in forested public land across CONUS. Trained surveyors estimate the percentage of dead trees per acre, viewing the forest from fixed-wing planes or helicopters. The surveyors draw polygons around the affected forest areas on maps and label each polygon as one of five classes of tree mortality: 1-3% (very light), 4-10% (light), 11-29% (moderate), 30-50% (severe), and greater than 50% (very severe). The polygons are then matched with ground surveys to assign the dominant beetle species to each, as these data are primarily used to track beetle outbreaks across CONUS. The resulting data is a set of irregularly-sized polygons labeled with the

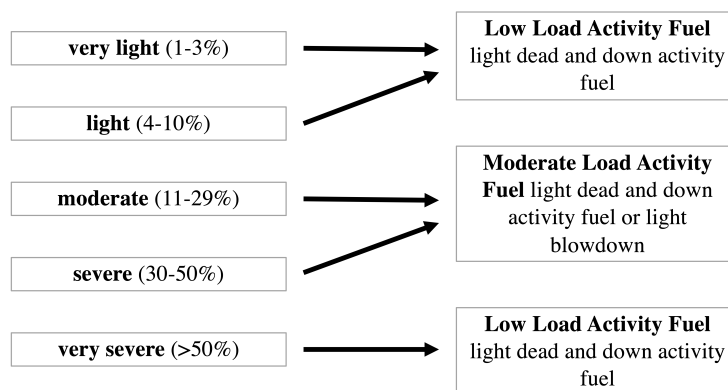
date of collection, the dominant beetle species, and level of tree mortality [11].

RF was chosen for this application due to its ability to handle both categorical and continuous variables and to capture complex interactions between several input variables [32]. Confusion matrices, accuracy scores, and hierarchies of feature importance may be used to confirm model accuracy and gain insight into feature dynamics. In particular, the Statistical Machine Intelligence and Learning Engine (Smile) version of RF was applied in Google Earth Engine. Google Earth Engine hosts a multi-petabyte library of geospatial data, and its code editor platform allows users to perform analyses over large amounts of data efficiently in the Cloud [65].

We created cloud-free composites of Sentinel-2 imagery from July 2019 (the month of the 2019 Colorado tree mortality survey), and September 2020 (just before the East Troublesome Fire). Following Meddens, Hicke, Vierling, and Hudak [91], we then calculated the chlorophyll red-edge index, shortwave infrared to near infrared ratio, tassell cap brightness, tassell cap greenness, and tassell cap wetness specific to the Sentinel-2 data. To develop training and validation data, we subset the tree mortality survey data to the fire event area (approximately 60km x 70km). We then generated 400 m<sup>2</sup> polygons randomly located within the tree mortality survey polygons, assigning them a label that mostly closely translates their USFS-IDS severity class to a representative Scott and Burgan fuel model (Figure 3.1). The *very light* and *light* tree mortality classes are labeled *low load*, the *moderate* and *severe* tree mortality classes are labeled *moderate load*, and the *very severe* tree mortality class is labeled *high load*. Each of the three resulting classes represents a fuel model in the slash-blowdown category of the Scott and Burgan fuel models, a category used to describe timber slash or downed fuel from wind damage. While ‘crosswalking’ fuel data to fuel models is a common practice [17, 123], it should be noted that it is a subjective process [79]. Effort was made to best match the USFS tree mortality classes to the fuel models based on the guidance for choosing representative fuel models provided in the original Scott and Burgan 40 fuel model publication [123]. To provide the RF model with data that captures all possible surface features within the wildfire domain, 400 m<sup>2</sup> polygons capturing healthy vegetation, bare ground, urban areas, and water comprise an additional class of other. Altogether, the RF model is provided multispectral,

C-SAR, and land cover class input in sample spaces labeled either *low load*, *moderate load*, *high load*, or *other*.

Figure 3.1: Insect and Disease Detection Survey (IDS) tree mortality classes mapped to Scott and Burgan 40 fuel models from the Slash-Blowdown class. Polygons from the IDS were mapped to their most representative fuel models using guidance from the original publication describing the fuel models.



The full set of polygons was split randomly into 70% for training and 30% for testing by class. The image bands, calculated indices, and land cover classes were sampled within the polygons. The RF classifier was run for the composite July 2019 image and tested for accuracy, before being applied to the September 2020 composite image. The model configuration that optimized accuracy of classifying the test dataset included 100 decision trees, 5 variables per node split, a minimum leaf population of 1, an unlimited maximum number of leaf nodes, and a bag fraction of 0.5. Once classified, the fuel layer is written in .tif format such that it may be analyzed using Python and utilized as input for a wildfire behavior model.

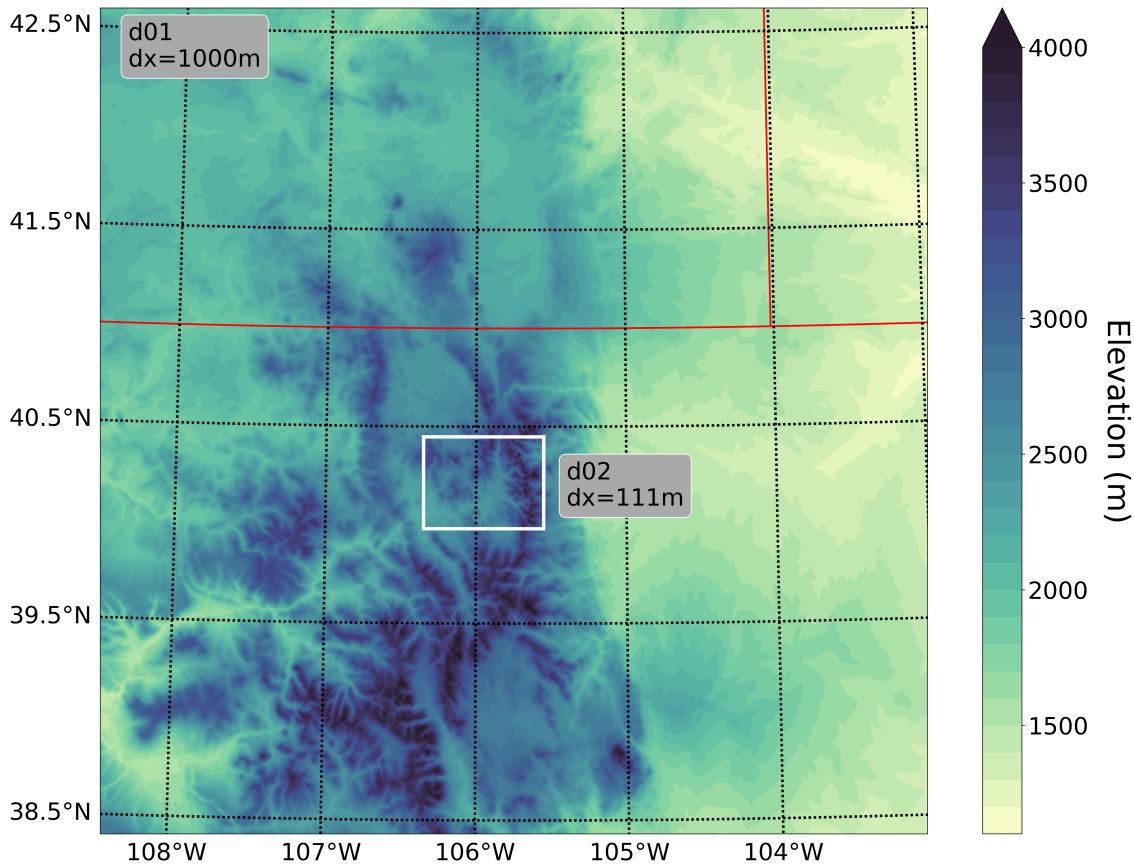
### 3.2.3 WRF-Fire

To examine the impact of the LANDFIRE fuel data on the evolution of the East Troublesome Fire, we used the Weather Research and Forecasting (WRF) model [124] coupled to a fire behavior model based on the Coupled Atmosphere-Wildland Fire Environment [42, 43]. The coupled model

is more commonly known as WRF-Fire [45]. In WRF-Fire, the meteorological grid is defined as in a typical WRF simulation; however, the fire grid is refined to compute finescale changes in the fuel properties and track the evolution of the fire perimeter via a level-set method [87, 98]. Using the Rothermel [116] parameterization, the winds, fuel characteristics, and terrain slope on the fire grid determine the fire rate of spread. Once a fire is ignited in the model, the burn rate of the fuel is determined via the parameterization developed by Albini [15], which computes the amount of heat and moisture released based on the fuel properties. The released energy then feeds back to the atmosphere such that there is full coupling between the fire and atmosphere.

Our simulations are conducted using a two-domain setup, with the outer (d01) and inner (d02) domains covering an area of approximately 220,000 km<sup>2</sup> and 32,000 km<sup>2</sup>, respectively (Figure 3.2). By and large, our chosen model physics and dynamics options follow the operational WRF-Fire modeling setup, called the Colorado Fire Prediction System, developed by the National Center for Atmospheric Research (NCAR). Options relevant to this study include: (i) a horizontal grid cell spacing of 1000 m and 111.11 m, respectively, on the meteorological grid in d01 and d02; (ii) a horizontal grid cell spacing of 27.77 m on the fire grid in d02 (subgrid ratio of 4 compared to the meteorological grid); (iii) 44 vertical grid cells in d01 and d02; and, (iv) activating the Mellor-Yamada-Nakanishi-Niino (MYNN) [100] planetary boundary layer (PBL) parameterization on d01, while d02 is run in large-eddy simulation (LES) mode. Furthermore, to determine the impact of meteorology on the wildfire evolution and bolster our results related to fuel model sensitivity, we test two different meteorological datasets used for initial and boundary condition forcing: the North American Mesoscale Forecast System (NAM) and the European Centre for Medium-Range Weather Forecasts Reanalysis v5 (ERA5).

Figure 3.2: The two-domain setup used in the WRF-Fire simulations. Terrain elevation is color contoured according to the colorbar (units in m) and state outlines are represented by the solid red lines.

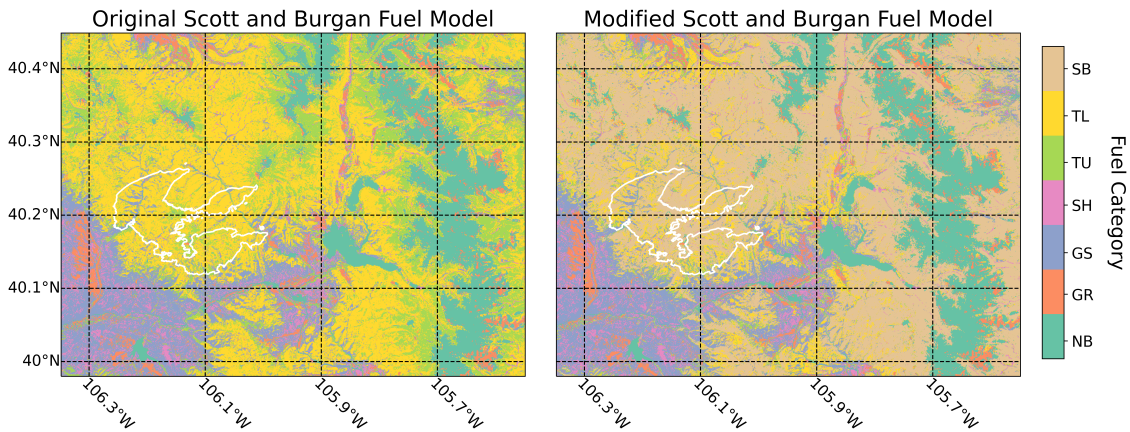


During the pre-processing step for WRF-Fire, the fuel categories of the Scott and Burgan 40 fuel class model are assigned to each fire grid cell. For the purposes of this study, we generate two different input files: one that contains the default Scott and Burgan 40 fuel class model and one that contains the modified Scott and Burgan 40 fuel class model following our RF results, as described above. We refer to the former simulation as Control and the latter simulation as ML (abbreviation for Modified Layer). The original and modified Scott and Burgan fuel model layers used in our WRF-Fire simulations are shown in Fig. 3.3. We also utilize the 3 arc second Shuttle Radar Topography Mission (SRTM) terrain data for the fuel grid. Recent developments by NCAR allow us to apply heterogeneous fuel moisture content (FMC) values to our fire domain [89]. As an

additional sensitivity test, we evaluate the impact of FMC by also conducting a simulation with constant FMC set to 9%, which is approximately equal to the domain-averaged value computed from the heterogeneous FMC data set (not shown).

In summary, we conduct a total of five simulations based on the various model sensitivities discussed above: (1) NAM Control, (2) NAM ML, (3) NAM ML + Constant FMC, (4) ERA5 Control, and (5) ERA5 ML. Each of our simulations begins at 21 October 2020, 1800 UTC and ends at 22 October 2020, 1500 UTC. The fire is ignited from an active perimeter (provided by the National Interagency Fire Center and shown in Fig. 3.3) measured at 22 October 2020, 0020 UTC (6 hours and 20 minutes after the simulation start time to ensure sufficient spin-up time). We now show results from the various WRF-Fire simulations to highlight the relative impact of varying the fuel categories, meteorological forcing data set, and FMC.

Figure 3.3: The original (left) and modified (right) Scott and Burgan fuel model layers used in the WRF-Fire simulations. The active fire perimeter used to initiate the simulations is shown in white. Fuel categories represent the fuel type of the fuel model; Slash-Blowdown (SB), Timber Litter (TL), Timber-Understory (TU), Shrub (SH), Grass-Shrub (GS), Grass (GR), and Nonburnable (NB)



### 3.3 Results

The RF algorithm correctly classified over 84% of the test data in the fire domain, and performed well at separating the tree mortality classes from the other class. The RF misclassified 6.1% of the *low load*, <1% of the *moderate load*, and 8.7% of the *high load* classes as *other*. The confusion matrix for the classifier’s performance on the test dataset is given in Table 3.1. Table 3.2 shows the precision (positive predictive value), recall (true positive rate), and F1-score (weighted average of precision and recall) for each class.

Table 3.1: Confusion matrix for the classifier’s performance on the test dataset.

	<b>other</b>	<b>low load</b>	<b>moderate load</b>	<b>high load</b>
<b>other</b>	8505	337	257	52
<b>low load</b>	31	256	120	105
<b>moderate load</b>	8	232	457	196
<b>high load</b>	38	148	179	72

Table 3.2: Precision, recall, and F1-scores for the classifier’s performance on the test dataset.

	<b>precision</b>	<b>recall</b>	<b>F1-score</b>
<b>other</b>	0.927	0.992	0.958
<b>low load</b>	0.520	0.252	0.340
<b>moderate load</b>	0.489	0.471	0.480
<b>high load</b>	0.162	0.157	0.160

The fuel updating process resulted in changing a significant amount of the *Timber Litter* and *Timber-Understorey* fuel classes in the original fuel model layer to *Slash-Blowdown* fuel classes in the

modified fuel layer. *Timber Litter* and *Timber-Understory* are fuel model classes in which the main fire carriers are litter such as pine needles or hardwood leaves shed from timber, and grasses, shrubs, litter and moss respectively. These are classes typically designated to healthy timber systems with finer fuels under the tree canopy. In the semi-arid climate of the East Troublesome Fire case study, the wildfire rate of spread generated from these fuel models is low to moderate. In contrast, the wildfire rate of spread resulting from the slash-blowdown fuel models is moderate to high.

The WRF-Fire results from all sensitivity simulations are shown for two observed times in Figure 3.4 and Figure 3.5, with time series of various burn area and burn rate statistics given in Figure 3.6. Table 3.3 summarizes the forecast and observed areas for each of the simulations.

Overall, WRF-Fire underpredicts the East Troublesome Fire burn area regardless of the model setup explored in this study. Nonetheless, we find that modifying the fuel layer has the largest, positive impact compared to modifying meteorological forcing data set or the FMC. Conducting simulations using the default Scott and Burgan fuel model (the fuel data that was available to incident commanders at the start time of the fire) results in a much more substantial underprediction of the fire's burned area compared to using the updated fuel layer. As a result, the burned area prediction better matches the observed burned area, shown visually in Figs. 3.4 and 3.5 and quantitatively in Fig. 3.6 and Table 3.3. Additionally, our results show that forcing WRF-Fire with NAM leads to better agreement with observations than when using ERA5, likely due to enhanced wind speeds in NAM (further explained below). For this particular case, the influence of FMC is very small compared to that of the fuel layer or meteorological forcing.

Figure 3.4: The sensitivity simulation results (solid yellow colorfill) using NAM meteorological data with the original fuel inputs, the modified fuel inputs, and the modified fuel inputs with a constant 8% fuel moisture content (labelled NAM Control, NAM ML, and NAM ML + Constant FMC respectively), and the simulations using ERA5 with the original fuel inputs and the modified fuel inputs (labelled ERA5 Control and ERA5 ML respectively). The observed fire perimeter (solid magenta line) was captured aerially at 06:40 UTC on 2020-10-22.

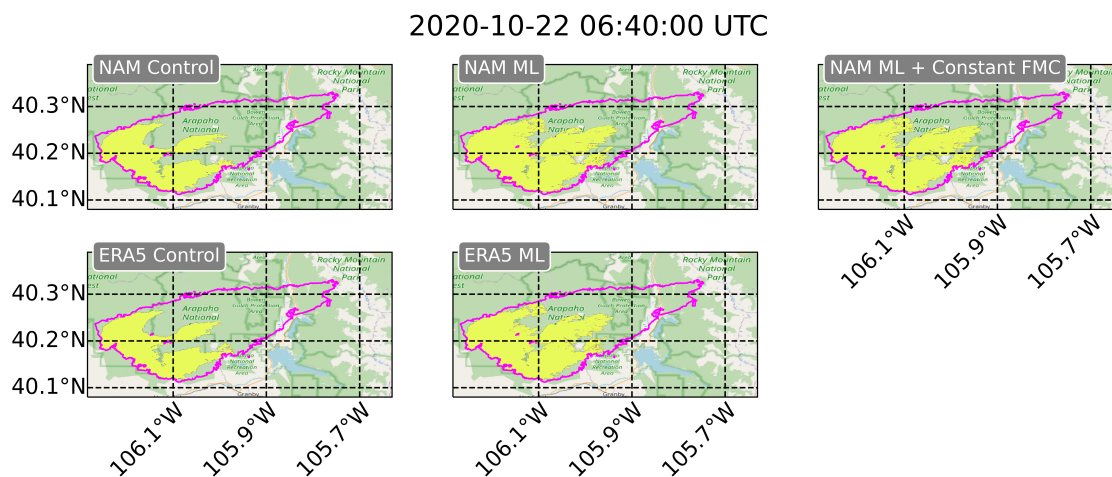


Figure 3.5: As in Figure 3.4, though for 0240 UTC on 10/23/2020.

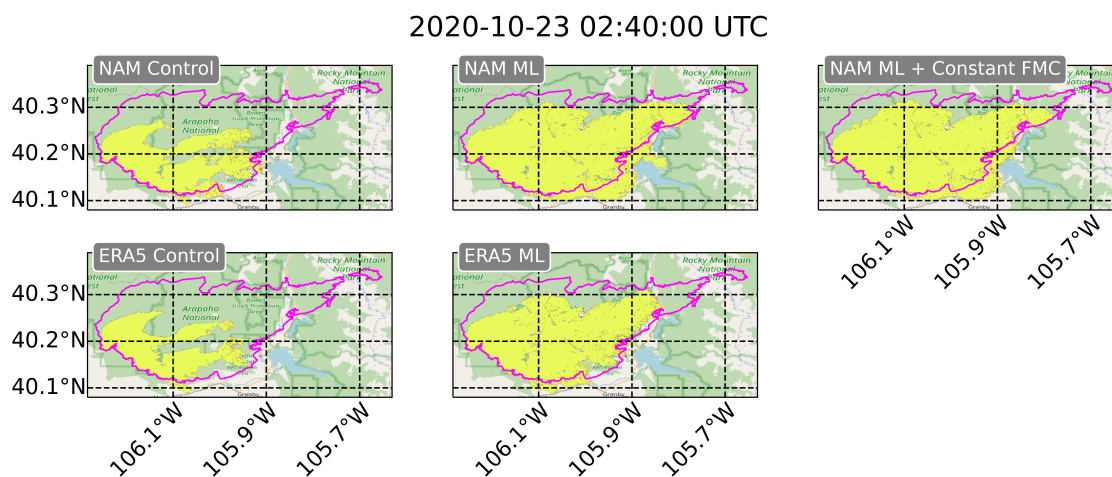


Figure 3.6: Time series of (a) burn area ( $\text{km}^2$ ), (b) burn area fraction (ratio of ML to Control), (c) burn rate ( $\text{km}^2 \text{ hr}^{-1}$ ), and (d) burn rate difference (ML minus Control). Model results are shown by the lines (according to the legend), while NIFC IR perimeters are shown in the magenta diamonds (labeled 'Obs' in the legend). The legend for panel (a) also applies to panel (c).

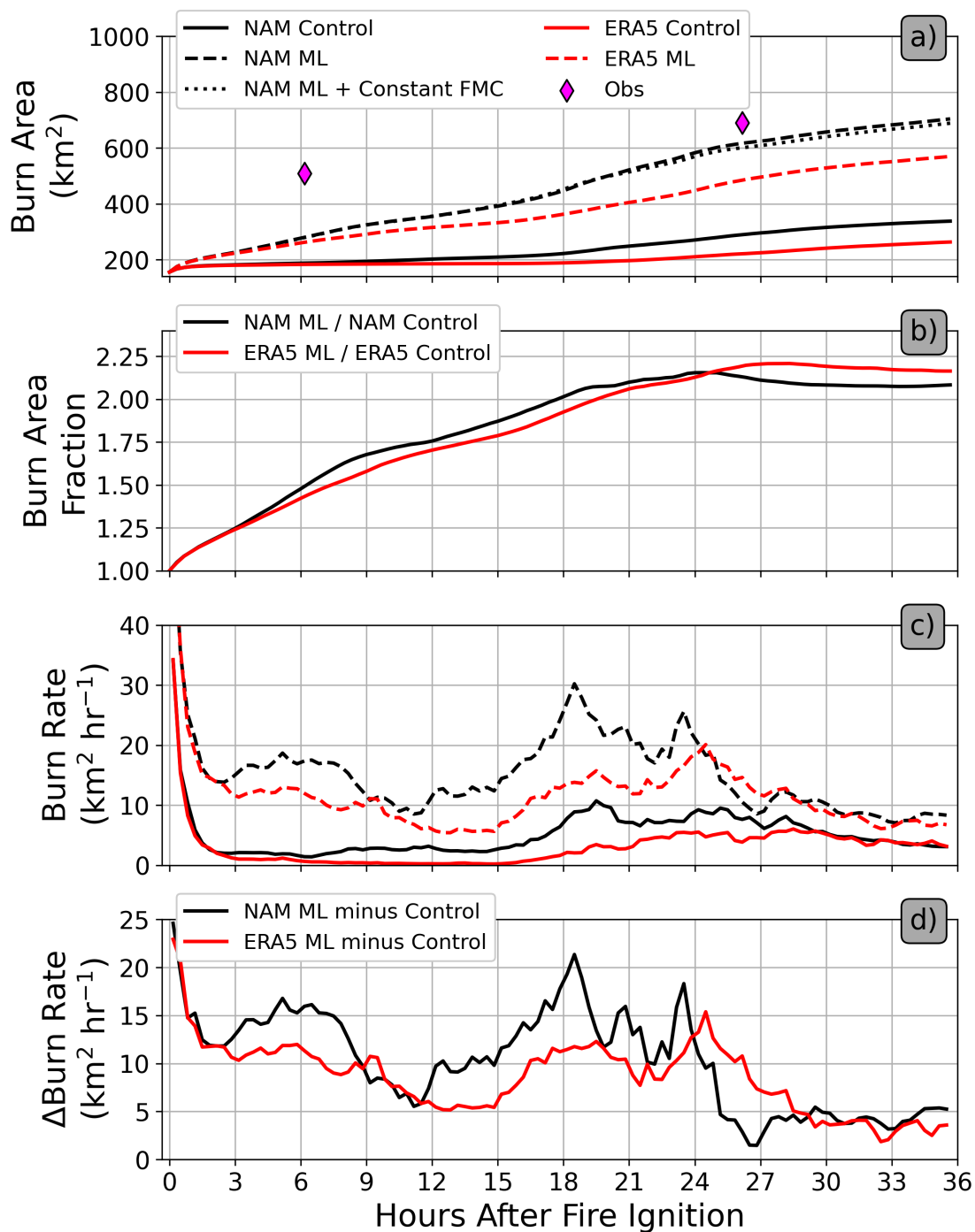
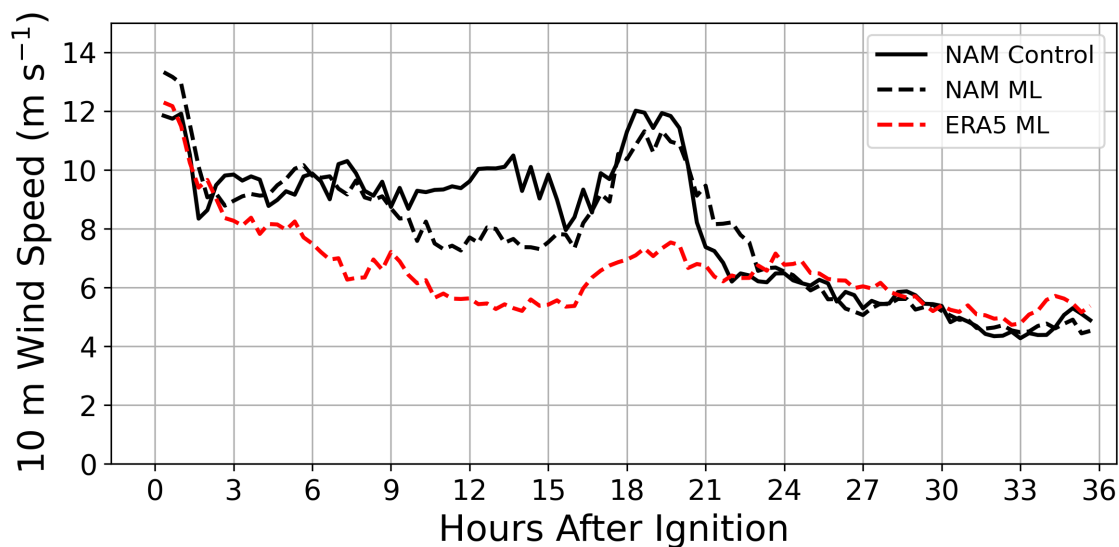


Table 3.3: Summary of the forecast burned area values, compared with observations occurring at the two timestamps within the simulation time frame. All forecast values in the table result from the simulations using NAM meteorological data.

<b>date</b>	<b>simulation</b>	<b>Forecast Area (km<sup>2</sup>)</b>	<b>Observed Area (km<sup>2</sup>)</b>	<b>Overlap Area (km<sup>2</sup>)</b>
10/22/20 0640 UTC	Control	188.92	508.59	179.62
	Updated Fuels	285.34	508.59	258.31
	Updated Fuels & constant FMC	284.63	508.59	259.04
10/23/20 0240 UTC	Control	293.87	689.57	272.17
	Updated Fuels	624.72	689.57	532.33
	Updated Fuels & constant FMC	608.39	689.57	531.15

A comparison of 10-m wind speeds along the fire front from the NAM Control, NAM ML, and ERA5 ML simulations are shown in Fig. 3.7. This figure shows that the low-level wind speeds are stronger in NAM ML compared to ERA5 ML supporting the notion that the WRF-Fire simulations with NAM initial and boundary condition forcing produce faster fire spread largely due to enhanced low-level wind speeds. In fact, the largest differences in the NAM ML and ERA5 ML lines correspond well with the largest difference in burn rate between NAM ML and ERA5 ML (Fig. 3.5c). Furthermore, we find that the 10-m fire front wind speeds are quite similar between NAM Control and NAM ML. This result suggest that the large differences in the burned area forecasts between the Control and ML simulations may be confidently attributed to the differences between the original and modified fuel model layers and the resultant differences in fuel properties.

Figure 3.7: Time series of fire front-averaged 10 m wind speed at model grid cells with active burning. We average across all horizontal grid cells where the fire rate-of-spread is  $> 0.05 \text{ m s}^{-1}$ . Results from three select simulations are shown according to the legend.



### 3.4 Discussion

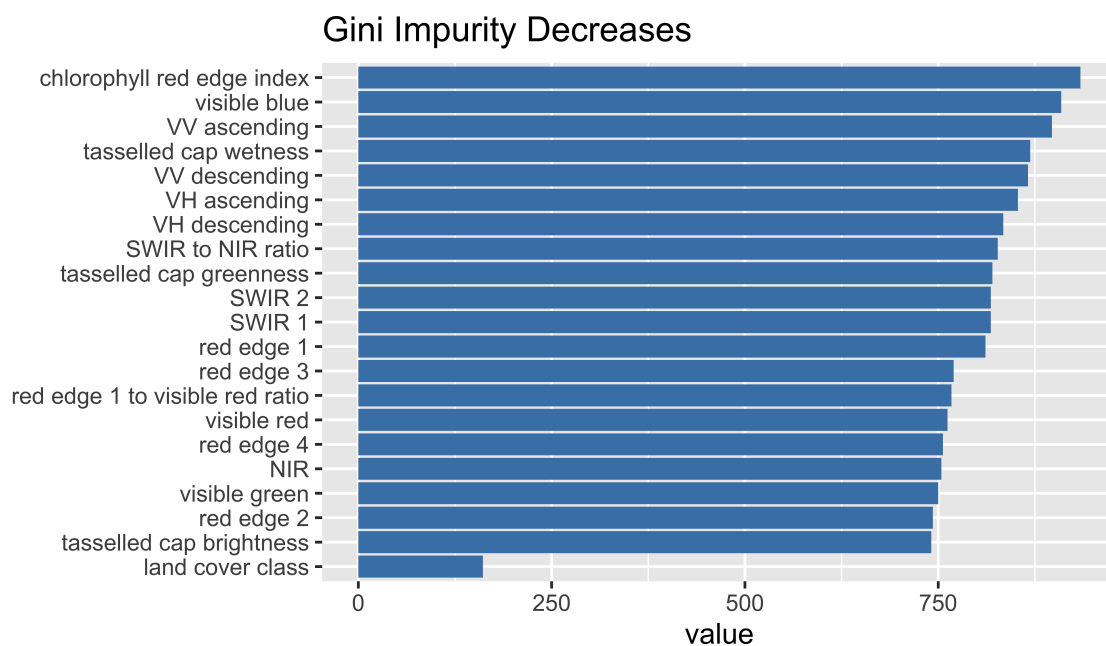
Examining the confusion matrix of the RF classifier output shows that the model correctly classifies approximately 92.7% of the other category correctly, most frequently mistaking it for the low class (4.2% of the time) in the test data set. 52% of the low class was correctly classified, and misclassified as the moderate class 21% of the time. The RF correctly classified 48.9% of the moderate class, mistaking it for the low class 28.8% of the time. Finally, the high class was correctly classified 16.2% of the time, while mistaken for the moderate class 41.2% of the time. This analysis shows that while the model performs well at distinguishing between the other class and the slash-blowdown classes, it has not been provided enough information to excel at classifying the different severity levels. This is likely due in part to uncertainty in the training data, particularly in the tree mortality surveys as the aerial collection practices are subjective in nature [47]. Similar issues may arise in applying this method to other scenarios, which highlights the importance of including ancillary data when available and understanding the limitations of any included datasets.

The data used to train the RF classifier and to classify images were chosen with the intent of

capturing information on tree mortality throughout the fire domain. In the context of a different set of known conditions, it would be necessary to choose data representative of those conditions. Regardless, the operator would need an understanding of available data and how it translates to on-the-ground conditions. Providing the RF classifier with additional information about the particular conditions just before a fire will likely improve classification accuracy when implemented mindfully.

The development and implementation of the RF in this study was performed in Google Earth Engine, which gives the Gini impurity decreases of each random forest node as a metric of feature importance. Examining the hierarchy of these values for the RF features shows that the chlorophyll red-edge index suggested by Meddens, Hicke, Vierling, and Hudak [91] is the most important feature (Figure 3.8). This index is particularly sensitive to chlorophyll, carotenoids, and anthocyanin production [64], which indicate vegetation senescence. There is an inevitable change in senescence simply due to the seasonal changes between July 2019 (the time of the tree mortality surveys) and September 2020 (the time just before the East Troublesome Fire). As the chlorophyll red-edge index is important to classification, senescence may be confounded with the intended classification of tree mortality in this case. However, the C-SAR bands, which contribute information on the surface texture and were intended to help distinguish between vegetation types and standing and downed timber, were also highly important to the classification. Given the high degree of classification accuracy, this indicates that collectively the input data provided was adequate to train the RF, and that any cells classified as tree mortality due to the signature of senescence are of minimal consequence.

Figure 3.8: The sum of the Gini impurity decreases across all node splits for each individual random forest feature. The bars represent the importance of each feature, measured through the sum of all the Gini impurity index decreases for each feature included in the random forest classifier.



Google Earth Engine runs in the Cloud and houses several relevant remote sensing data sets. Based on the methodology described in this study, it would be possible to develop an operational system that provides fuel updates in real time on an on-demand basis, and which would be available to fire behavior analysts and incident commanders. We would advise becoming familiar with the available data sets that are most relevant to the region being simulated. Moving forward more remote sensing data will become available, and may be used fruitfully for this purpose. Two additional Sentinel-1 satellites, both equipped with C-SAR instrumentation, are scheduled for launch in 2022 and 2023, and are expected to shorten the current revisit time for the system. One additional Sentinel-2 satellite is scheduled for launch in 2024, and will likewise shorten the revisit time and contribute multispectral imagery to the already established Sentinel-2 system. The fuel model data currently available provides a solid foundation for mindfully adjusting fuel layers prior to running simulations using wildfire behavior models. The incoming wealth of remote sensing data and modeling tools will only provide more opportunity for refreshing this data as needed.

### 3.5 Conclusion

This work presents an effective workflow for updating fuel data used in wildland fire behavior modeling. It builds on available fuel data and provides a solution to quantifying fuel characteristics in an accurate and timely manner. While the East Troublesome case study focuses on dead, downed timber due to beetle infestation and wind events, the workflow presented here may be applied to several types of disturbance events that affect wildland fire fuels, given the availability of relevant data. These methods were intentionally developed using freely available data and the analysis and modeling platform, Google Earth Engine to make them accessible to a broad user base, including wildland fire researchers and incident commanders. We anticipate that with the increase in wildland fire activity, research, and response, as well as the increase in availability of remotely-sensed data, that these methods will aid in improving wildland fire forecasts.

## Chapter 4

### Regional-Scale Drivers of Daily Fire Growth Across the Contiguous United States

#### 4.1 Introduction

From the chaparral ecosystems and Santa Ana winds of California to the conifer forests and steep slopes of the Rocky Mountains, the United States varies greatly in combinations of wildland fire drivers. As such, we see a diverse range of fire behavior across the contiguous United States (CONUS). Several studies have investigated the physical mechanisms of fire growth in laboratory experiments [118, 37, 18, 61, 19, 56]. Significant research has also been done to investigate the drivers of fire growth at the event scale [46, 75]. However, very little is known about continental and regional-scale drivers of day-to-day fire growth.

Small-scale experiments within labs and prescribed burns focused on the interaction of fuels, heat and oxygen have shown that temperature directly affects fire behavior through heat requirements for ignition. Fuels that are already warm need less energy to ignite. Fuels exposed to sunlight will be warmer and drier than fuels in the shade, directly affecting fire rate of spread. Likewise, fuels are typically warmer during mid-day than in the morning, evening, and nighttime. Rising temperatures during the day decrease the relative humidity and fuel moisture [77]. Relative humidity has a direct, positive relationship with fuel moisture [77], and fluctuates throughout the day with more moisture in the coolness of the morning and evenings, less moisture during the heat of the mid-day. Moreso, precipitation has an immediate and direct effect on fuel moisture [57], and a suppressing effect on active fire.

Other experiments have focused on fire regimes through long-term or large-scale investigation of ignition, vegetation, and climate. Recent studies have shown climate change has shifted fuel characteristics by changing the suitability of the environment and the mechanisms that determine the rise and fall of species populations [14, 31]. For example, the deserts of the Western United States (U.S.) are likely to see a difference in the spread of invasive grasses due to (human-caused) climate change. Cold-intolerant grasses benefit from a longer freeze-free season (shorter winter). Warmer temperatures lengthen the fire season, and the earlier onset of fires bring conditions that exaggerate the fire-invasive feedback loop [14]. In tropical climates, climate-induced droughts decrease photosynthesis, and increase tree mortality and autotrophic respiration (a large source of  $\text{CO}_2$ ), promoting wildfire by providing available fuel in a previously fuel-limited system [31]. Larger, more frequent fires in these forests result in more greenhouse gasses being released in large quantities, magnifying climate change [29]. There is also a temporal correlation between human-caused and lightning-caused fires from year to year, suggesting that the total number of fires that propagate is largely dependent on the fuel and meteorological conditions. Those conditions are becoming more favorable for fire propagation with climate change [23].

While this research has propelled our understanding of wildland fire and its drivers at small and large scales, there is room to investigate the combination of daily fire growth at a continental scale. In this research we ask, what are the key drivers of daily fire spread across CONUS, and how do they differ across ecoregions? Previous research on fire behavior at a continental scale was limited by the lack of a long-term record of daily fire growth. We paired a twenty-year record of daily fire progressions for over tens of thousands of events, across CONUS with weather, fuel, and terrain information to assess the drivers of fire area increase on a daily time scale. To determine the most important drivers for each region, we developed a set of random forest models for each of ten ecoregions estimating the daily burned area increase as well as the peak burned area increase (the largest daily area increase for each event). We used each model's feature importance values determined through permutations to define the hierarchy of drivers for each region across CONUS.

## 4.2 Methods

### 4.2.1 Dataset

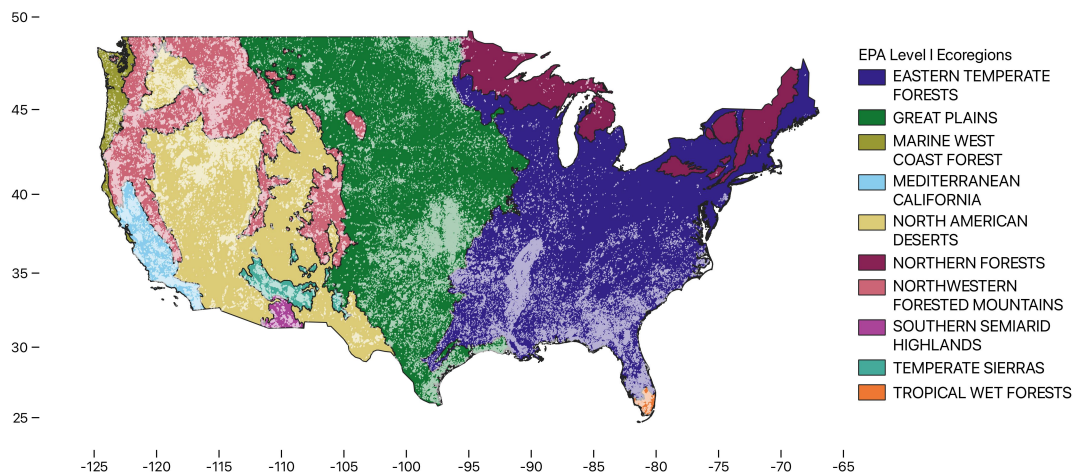
#### 4.2.1.1 FIRED daily burn area

To capture daily burn area by fire event across a twenty-year record, we used data resulting from the Fire Events Delineation (FIRED) algorithm developed by Balch et al. (2020) [24]. The FIRED algorithm clusters “burned” pixels in the MODIS MCD64 Burned Area Product [63] that are close together in space and time in order to delineate fire events across CONUS. The dataset used in this research was generated using a spatial parameter of 5 pixels, and a temporal window of 11 days. These parameters were determined through matching Monitoring Trends in Burn Severity (MTBS) fire events with the burned area pixels from MODIS MCD64 [24]. The resulting data set includes  $x$  fire events, each with active fire perimeters at a daily timescale, spanning November 2001 through March 2021.

#### 4.2.1.2 Environmental Protection Agency Level I Ecoregions

The FIRED dataset was subset by the Environmental Protection Agency (EPA) Level I Ecoregions. The Level I ecoregions were developed in 1987 through pattern analysis incorporating the spatial correlation of physical and biological factors [101, 102]. These factors include geography, land use, hydrology, vegetation, climate, soils, physiography and wildlife. Other levels (II, III, and IV) exhibiting finer granularity in their distinctive features are nested within the Level I ecoregions, meaning that in the hierarchy of the ecoregions, it is the broadest distinction between physical and biological factors in the United States. Level I includes 15 ecoregions, 10 of which intersect the FIRED dataset in the Continental United States (CONUS). Dividing the analysis by ecoregions allows for generalizations to be made about wildfire behavior at a regional scale. The CONUS EPA Level I Ecoregions and FIRED daily growth areas are shown in Figure 4.1

Figure 4.1: EPA Level I Ecoregions subset to CONUS with the FIRED daily burned area polygons shown in white.



#### 4.2.1.3 Drivers Dataset

Daily perimeters from each fire event were paired with data describing the meteorological conditions, terrain, and fuel characteristics present. The wind speed and wind direction provide the wind conditions across each daily burned area. 100-hr and 1000-hr fuel moisture content represent the amount of water in the vegetation present [12]. Vapor Pressure Deficit (vpd) is an absolute measure of the moisture deficit of the atmosphere, and is closely related to water stress on vegetation [12]. The Palmer Drought Severity Index is a regional drought index representing the severity of drought episodes [12]. Elevation, aspect, and slope provide information on the terrain [62]. The Rumple Index, the ratio of surface and projected area, provides information on the terrain complexity. The Multi-Scale Topographic Position Index (mTPI) distinguishes between ridges and valleys [136]. The Continuous Heat-Insolation Load Index (CHILI) provides a proxy

for the effects of insulation and topographic shading on evapotranspiration [136]. Physiographic Diversity provides information on land facet patterns within each daily burned area [136]. Each regional dataset was compiled in Google Earth Engine [65].

#### 4.2.2 Random Forest Regression Model

Two individual random forest models were fit to each ecoregion's dataset, one to estimate the overall daily fire growth, and one to estimate the peak burn days' fire growth (defined as the day with the maximum area of growth for each fire event). This allows a comparison between the drivers of daily fire growth and the drivers during the day when each fire event grew the most. The main wildfire behavior drivers for each model in each ecoregion were determined as the drivers with the greatest permutation feature importances. The permutation feature importances help to identify the main wildfire behavior drivers for each model in each ecoregion. Feature importance is measured by observing the effect on model accuracy through randomly shuffling each predictor variable. The mean decrease in impurity importance of a feature is computed by measuring how effective the feature is at reducing variance when creating decision trees within random forest regression models. This method can be informative only if the features are independent of each other. If two or more features are collinear, their importance is split. So, care was taken to remove highly correlated features by examining a correlation matrix of all features. Table 4.1 gives the features used, along with their spatial scale, the metric used (mean, mode, variance, standard deviation), units and data source. Categorical features were represented through one-hot encoding, a method of representing each category as a binary value. Hyperparameters were selected through cross validation to optimize the model fit. The coefficient of determination ( $R^2$ ), mean absolute error (MAE) and mean standard error were used to assess the accuracy of each model. Partial dependence plots show how each of the most important features relate to the models' predictive capability, and scatter plots show the relationship between the important features and the predicted variables. Models were developed and implemented in Python's Sci-Kit Learn library [107].

Table 4.1: Data, spatial scale, metric, units, source, and description of the data used to describe fire drivers. Datasets were used as features within random forest regression models trained to estimate daily fire growth and peak fire growth within the EPA Level I Ecoregions across CONUS.

data	spatial scale	metric	units	source	description
aspect	10.2m	weighted mean	deg	USGS 3DEP National Map	weighted average aspect in the burned area
Continuous Heat-Insolation Load Index	90 m	weighted mean	-	Conservation Science Partners product, JAXA's ALOS DEM	represents the effects of insolation and topographic shading on evapotranspiration
date	-	-	-	FIRED	day of the year
100-hour fuel moisture	4638.3 m	weighted mean	pct	GRIDMET	weighted average ignitability of fuels 1-3" in diameter and moisture of fuels $\frac{3}{4}$ -4" below surface
Level III ecoregions	-	mode	-	EPA	the dominant Level III Ecoregion, a representation of subregions within each Level I ecoregion
Multi-Scale Topographic Position Index	270 m	mode	m	Conservation Science Partners, JAXA's ALOS DEM	represents the dominant landform
Palmer Drought Severity Index	4638.3 m	weighted mean	-	GRIDMET Drought	represents the severity of drought episodes (level of moisture) in each burned area
Physiographic diversity	270 m	weighted mean, variance	-	Conservation Science Partners	represents the land facet patterns within each burned area

Slope	10.2 m	weighted mean	deg	USGS 3DEP National Map	weighted average slope in the daily burned area
Vapor Pressure Deficit	4638.3 m	weighted mean	kPa	GRIDMET	represents the moisture deficit of the atmosphere, and water stress on vegetation
Wind direction	4638.3 m	weighted mean	deg	GRIDMET	weighted average wind direction in each burned area
Wind speed	4638.3 m	weighted mean	m/s	GRIDMET	weighted average wind velocity at 10m height in each burned area

### 4.3 Results

The variance in physiographic diversity is important to the model fit for the full set of burned areas and the peak burn days for all of the ecoregions. The range of daily growth generally decreases as physiographic diversity increases, and the presence of high physiographic diversity variance is particularly important for skillful model predictions of daily growth as evidenced by partial dependence plots.

Aside from the variance of physiographic diversity, other important features vary by ecoregion and the models fit for either burned area or peak burned area. Notable (highest ranking) features are discussed by ecoregion below.

#### 4.3.1 Marine West Coast Forests

The EPA Level III ecoregions are important to the model fit for the Marine West Coast Forests. The partial dependence plot shows that the model fit relies heavily on the *California Coastal Sage, Chaparral, and Oak Woodlands* and *Cascades* Level III ecoregions, but does not rely heavily on the *Coast Range, Klamath Mountains, Willamette Valley, Strait Of Georgia/Puget Lowland*, and *North Cascades*. The Level III ecoregions were not important to the model fit for

peak burned areas, the only notable feature in the model fit being physiographic diversity variance. Figure 4.2 shows the permutation feature importances for the features included in the random forest regression model estimating daily fire growth for the EPA Level I Marine West Coast Forest Ecoregion. Figure 4.3 shows the partial dependence plot for the model's EPA Level III Ecoregions feature and Daily Fire Growth.

Figure 4.2: The EPA Level III Ecoregions are important to the random forest regression model fit for the Marine West Coast Forest Ecoregion.

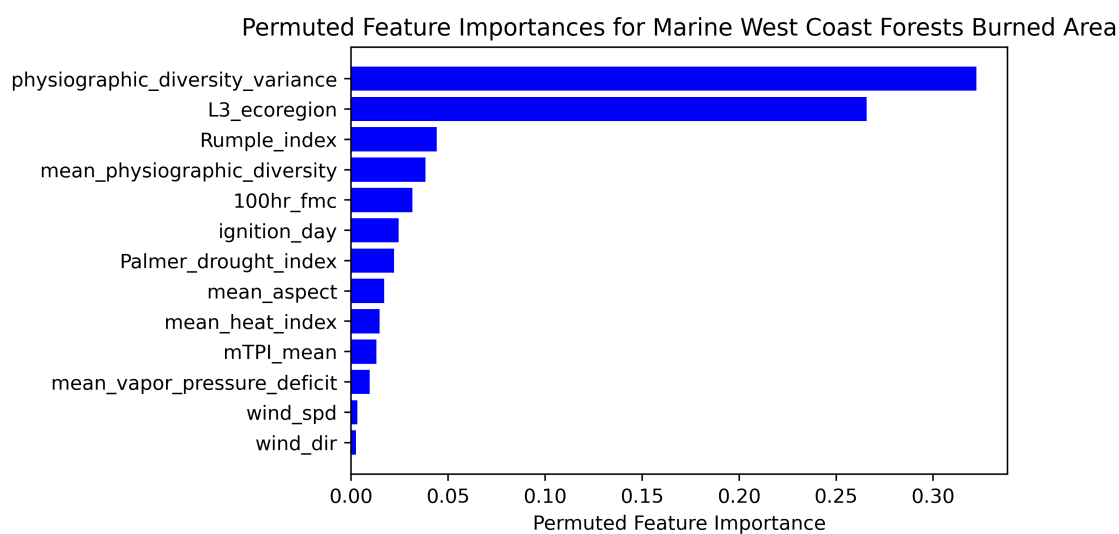
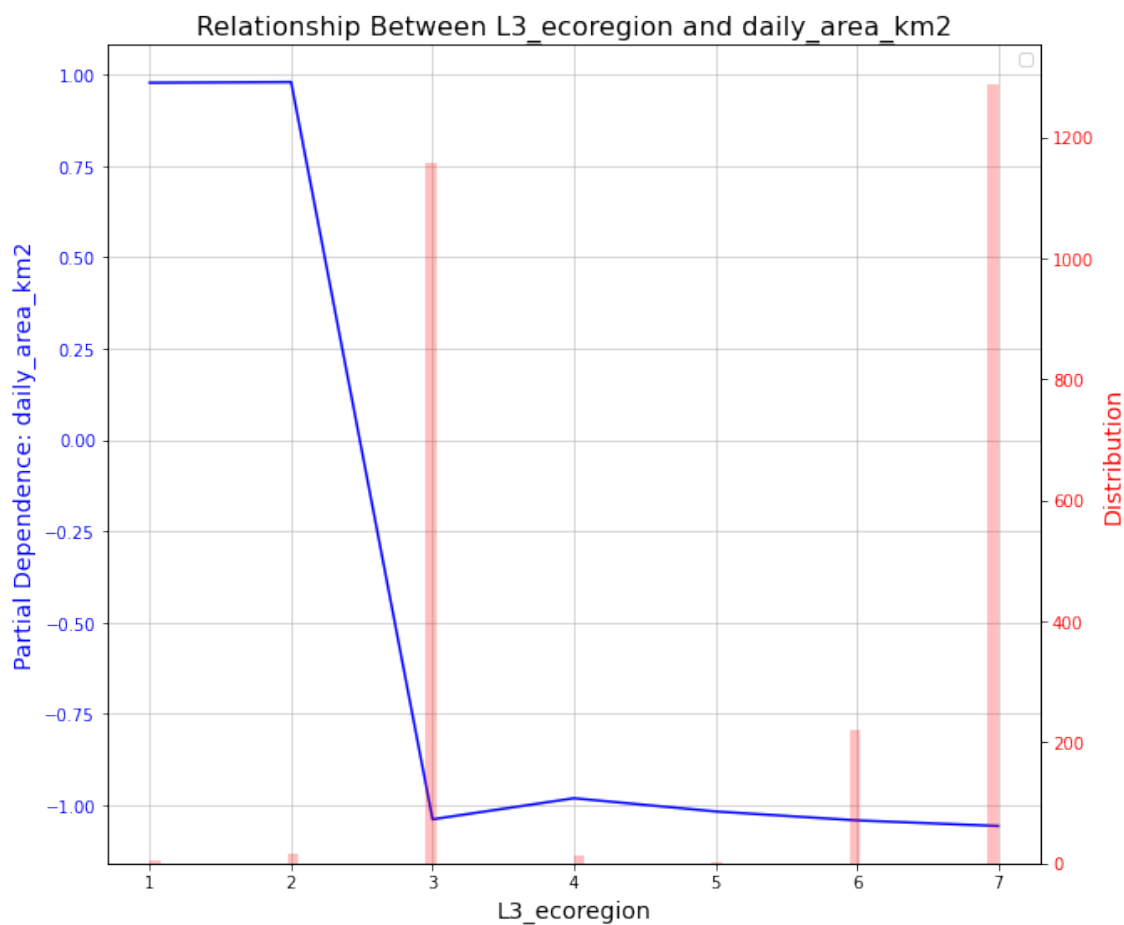


Figure 4.3: The random forest regression model fit for the Marine West Coast Forest Ecoregion relies heavily on the *California Coastal Sage, Chaparral, and Oak Woodlands* and *Cascades* Level III ecoregions.



### 4.3.2 Mediterranean California

The Rumple Index, a metric of terrain complexity, is important to the model fit for the Mediterranean California Level I ecoregion. The model fit becomes more important as the complexity of the terrain increases. Figure 4.4 shows the permutation feature importances for the features included in the random forest regression model estimating daily fire growth for the EPA Level I Mediterranean California Ecoregion. Figure 4.5 shows the partial dependence plot for the model's Rumple Index feature and Daily Fire Growth.

Figure 4.4: The Rumple Index is important to the random forest regression model fit for the Mediterranean California Ecoregion.

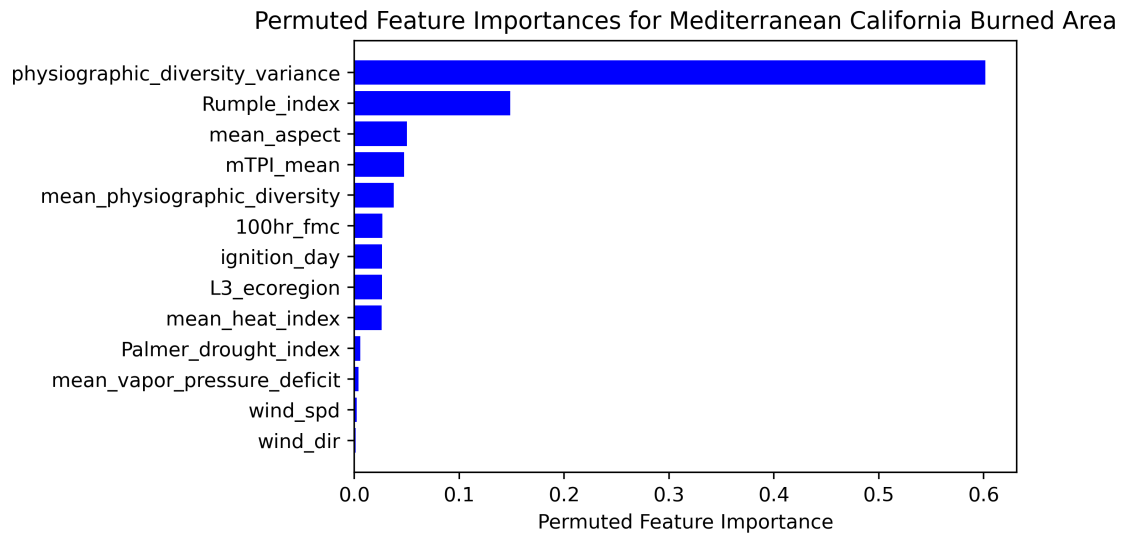
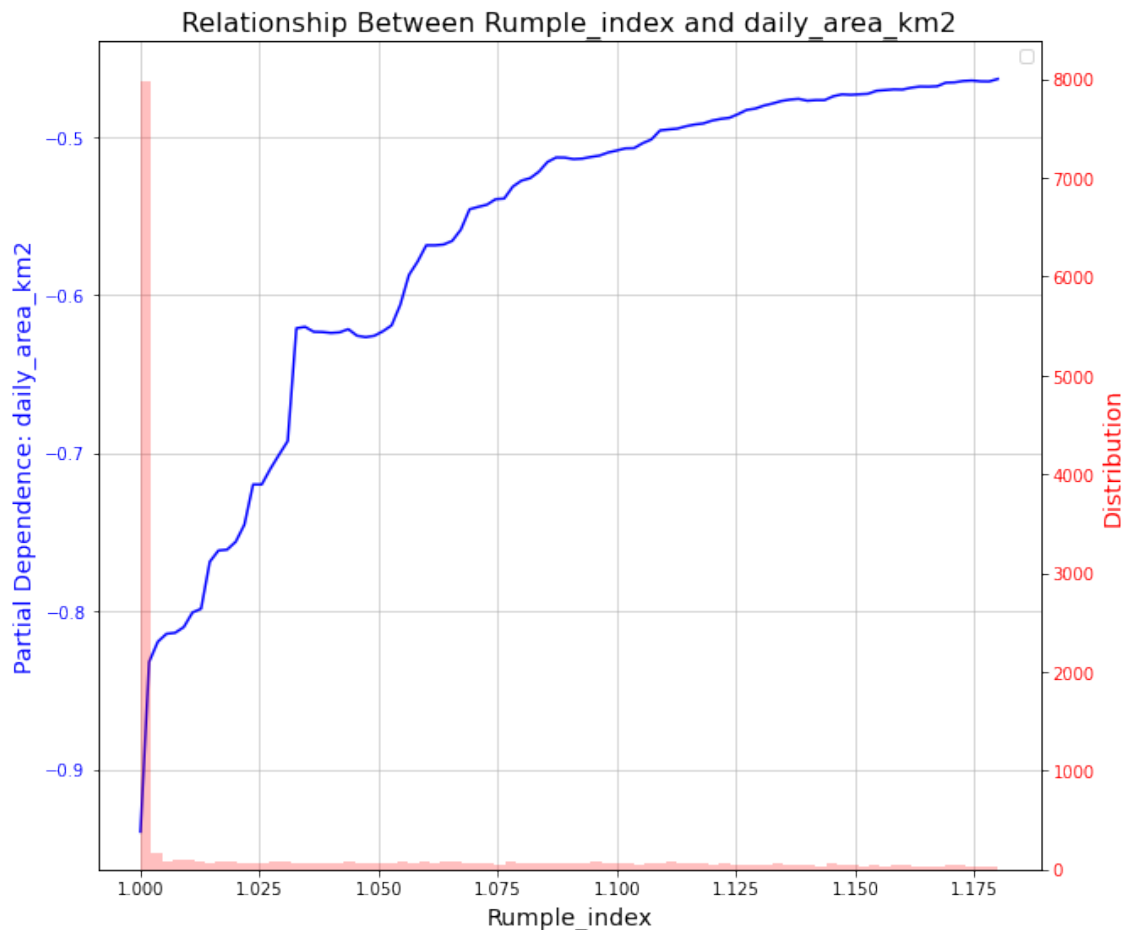


Figure 4.5: The random forest regression model fit for the Mediterranean California Ecoregion relies heavily on the higher values of the Rumple Index.



The Rumple Index was also an important feature in the model fit for peak daily fire growth in the Mediterranean California ecoregion. Here the values for the Rumple Index are slightly more compressed, but show a similar relationship to the daily fire growth model's partial dependence. Figure 4.6 shows the permutation feature importances for the features included in the random forest regression model estimating peak daily fire growth for the EPA Level I Mediterranean California Ecoregion. Figure 4.7 shows the partial dependence plot for the model's Rumple Index feature and Peak Daily Fire Growth.

Figure 4.6: The Rumple Index is important to the random forest regression model fit for the Mediterranean California Ecoregion.

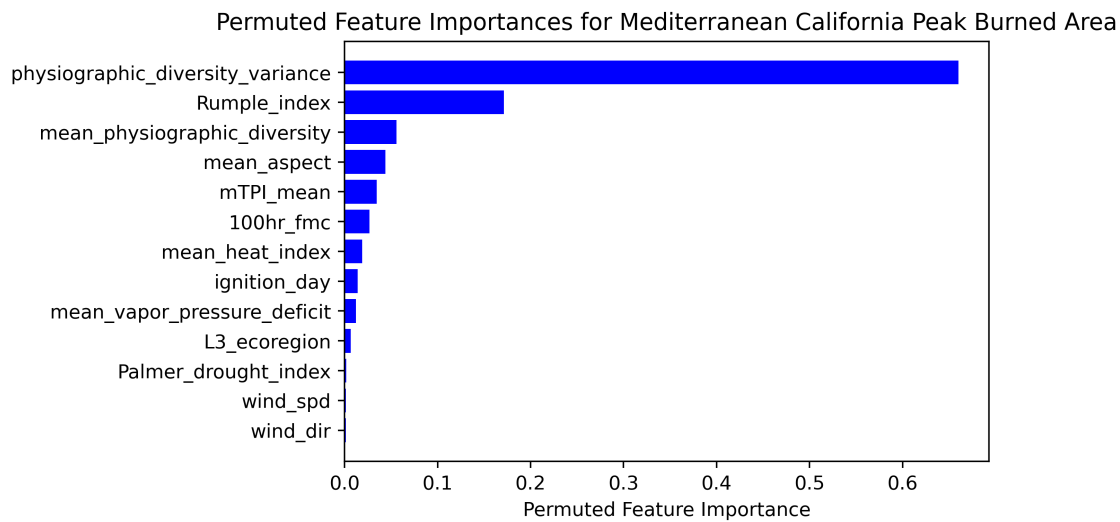
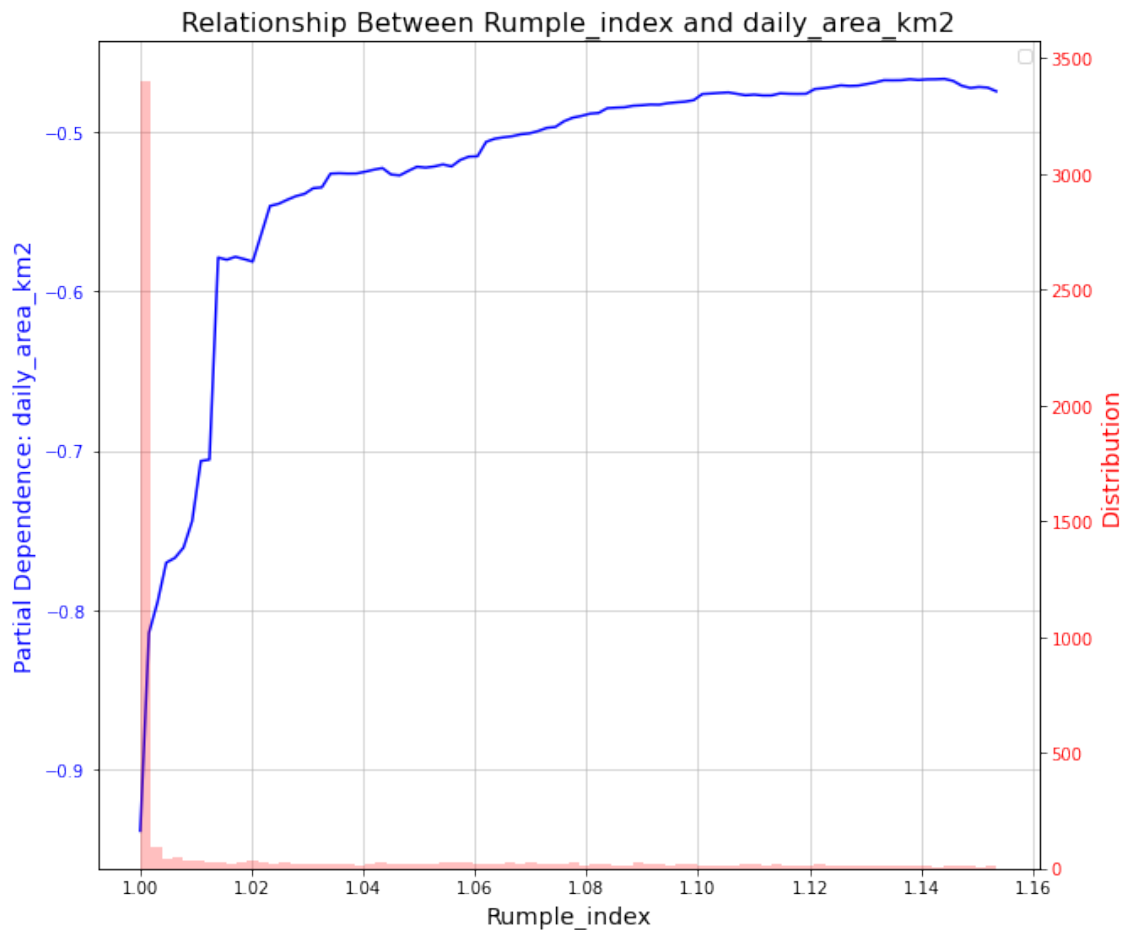


Figure 4.7: The random forest regression model fit for the Mediterranean California Ecoregion relies heavily on the higher values of the Rumple Index.



### 4.3.3 Tropical Wet Forests

The Rumple Index is also important to the model fit for Tropical Wet Forests, though here the range of values is much more compact, and the model fit becomes less dependent for values higher than 1.001. Figure 4.8 shows the permutation feature importances for the features included in the random forest regression model estimating daily fire growth for the EPA Level I Tropical Wet Forests Ecoregion. Figure 4.9 shows the partial dependence plot for the model's Rumple Index feature and Daily Fire Growth.

Figure 4.8: The Rumple Index is important to the random forest regression model fit for the Tropical Wet Forests Ecoregion.

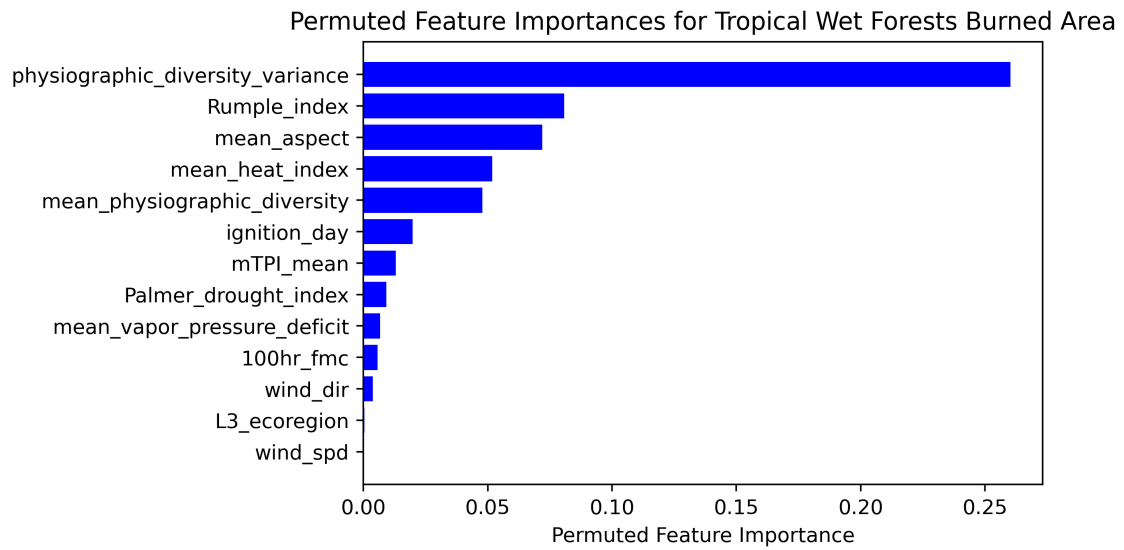
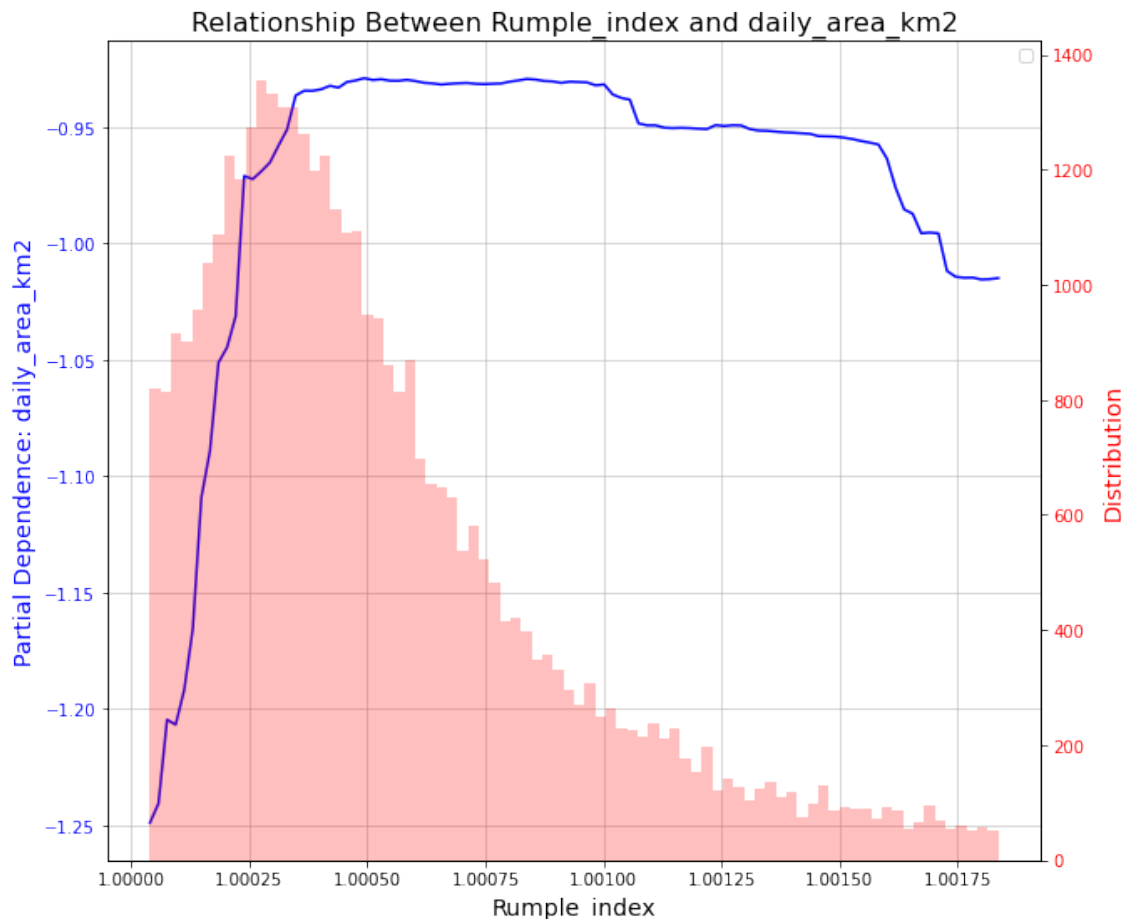


Figure 4.9: The random forest regression model fit for the Tropical Wet Forests Ecoregion relies heavily on the higher values of the Rumple Index.



In the model fit to peak burned area in the Tropical Wet Forests ecoregion, the Rumple Index is still important to model fit. Again, the model fit becomes less dependent for values higher than 1.001. Figure 4.10 shows the permutation feature importances for the features included in the random forest regression model estimating peak daily fire growth for the EPA Level I Tropical Wet Forests Ecoregion. Figure 4.11 shows the partial dependence plot for the model's Rumple Index feature and Peak Daily Fire Growth.

Figure 4.10: The Rumple Index is important to the random forest regression model fit for the Mediterranean California Ecoregion.

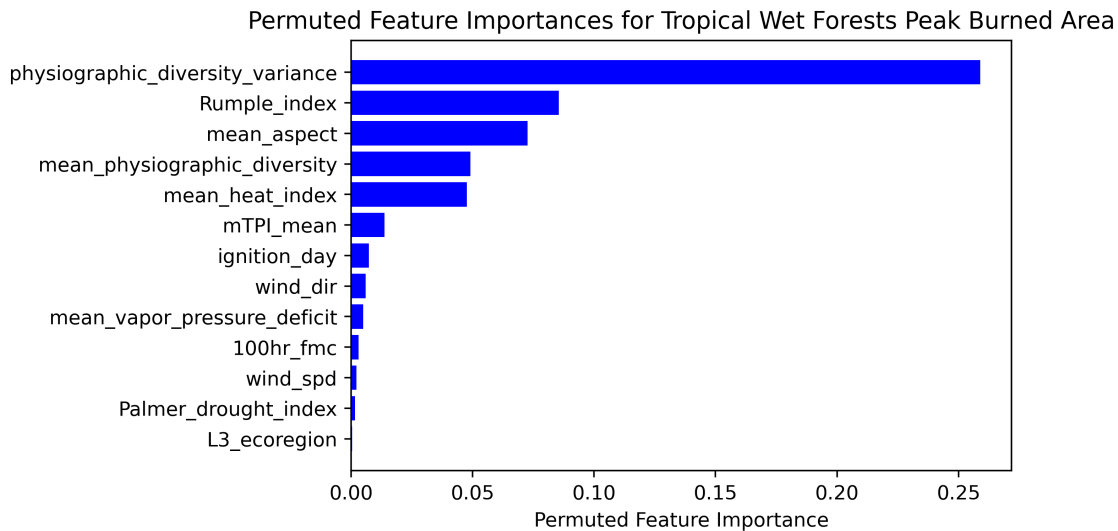
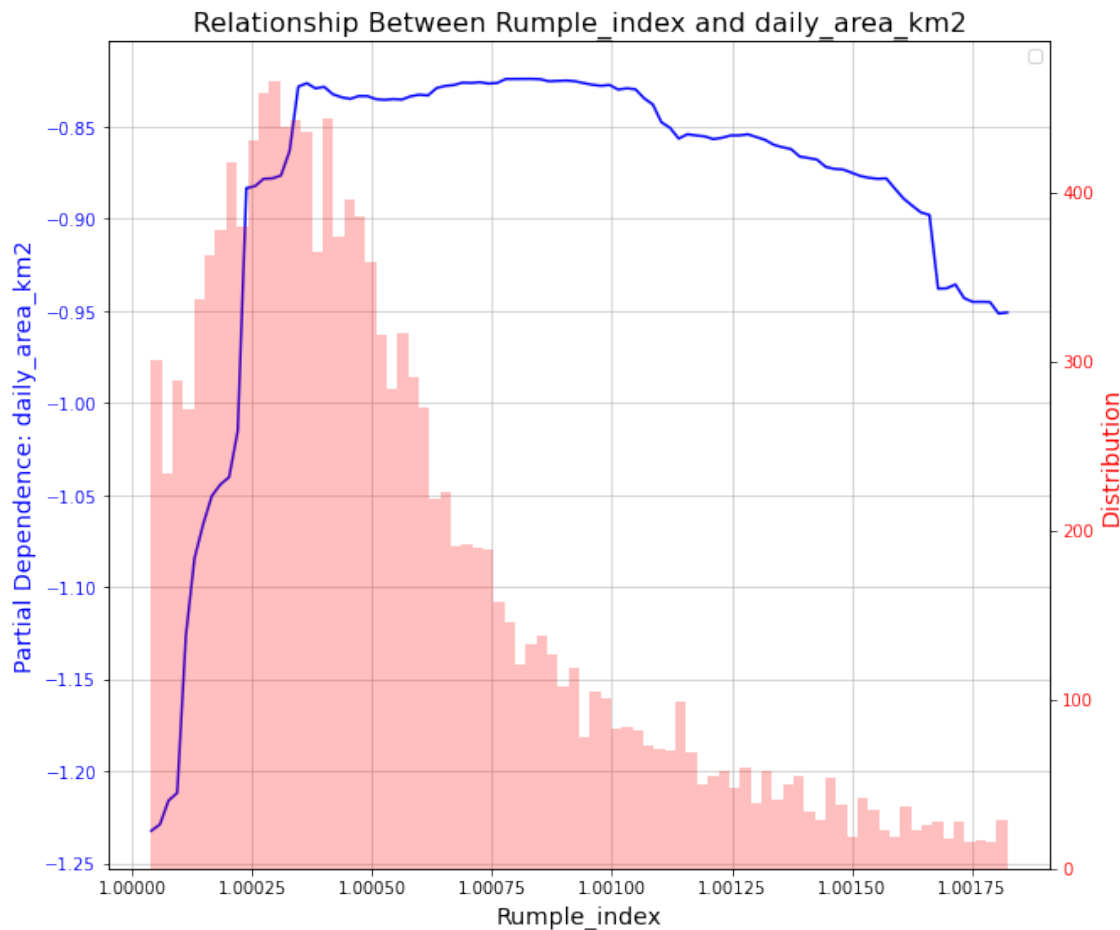


Figure 4.11: The random forest regression model fit for the Tropical Wet Forests Ecoregion relies heavily on the higher values of the Rumple Index.



#### 4.4 Discussion

The results show that the variance of physiographic diversity is an important driver of daily wildland fire growth across CONUS. The data for this feature in the set of random forest models originates from the physiographic diversity dataset developed by Theobald et al. (2015) [136]. A diversity index value is assigned to each 270 m grid cell in their dataset based on landforms (natural features of the earth's surface), estimates of incident radiation and heat load, and lithology (i.e. mineralogical and chemical composition of rocks and soil). High index values represent high levels of physiographic diversity, low index values signify little physiographic diversity. The variance of the physiographic diversity index value within each daily fire growth area represents the dispersion

of values from the mean value, a metric of the overall heterogeneity of physiographic diversity. High values of the physiographic diversity variance represent the daily fire growth areas with a high amount of environmental heterogeneity, low values represent daily fire growth areas that are more homogeneous in their overall physiography.

A wide range of daily growth values occur within the spaces that are environmentally homogeneous (low values of physiographic diversity variance). That is to say daily growth may be large, small, or in between in spaces that are physiographically homogeneous, where the surface features are somewhat uniform. However, high values of daily growth are less and less likely as the environmental heterogeneity increases (high values of physiographic diversity variance). This indicates that daily growth is inhibited in complex landscapes where the land features are varied, and diverse rock and soil compositions support a variety of vegetation patterns.

These results coincide with what we know to be true about wildland fire behavior. Weather, fuel, and terrain are considered the three broad categories of features driving wildland fire behavior at a daily temporal scale [116]. The variance of physiographic diversity lives within the terrain category, though it certainly bridges and interacts with weather and fuel. Indirectly, terrain influences fire spread through fuel moisture, vegetation composition, and continuity [114, 134, 126]. Slope directly affects fire behavior through preheating; energy transfer from the flaming front to upslope fuels accelerates fire spread [117]. South-facing slopes receive more energy and warmth from sunlight, in turn affecting fuel moisture quantity through evaporation, which in turn influences fuel quantity. Namely, fuel moisture and fuel quantity may be greater on the north vs. south facing slopes [114].

The heterogeneity, or texture, of the terrain influences both the flow of winds and the presence of natural barriers. Wind is deflected over mountains and ridges, flows through ravines, funnels into saddles, and bursts out of box canyons. The interface between contrasting aspects will be natural fire spread barriers [70, 58, 59], as are lakes, swamps, roads, burn scars, and spaces generally devoid of fuels.

While these results are consistent for the Level I ecoregions across CONUS, smaller subregions

are likely to have their own unique drivers. The ecoregions with additional important drivers were among the smallest ecoregion spaces. That is, out of the ten Level I ecoregions that intersect CONUS and the FIRED dataset, the Marine West Coast Forests, Mediterranean California, and Tropical Wet Forests cover comparatively smaller spaces. The random forest models for these ecoregions are highlighting additional important features because the features and daily fire area represented in their respective datasets are less broad. This indicates that dividing the dataset into smaller subregions, perhaps the Level II ecoregions, will scale the models in a way that captures regional variability across CONUS, and will result in determining specific drivers for each ecoregion. In Southern California for example, where Santa Ana winds are present, we would expect wind speed would be a main driver. In the Pacific Northwest, a climate-limited system, the main wildfire drivers are expected to be moisture-related variables such as vapor pressure deficit, fuel moisture, and drought index. The main drivers of fuel-limited systems in the Western United States are expected to be fuel-related; again, physiographic diversity as well as the Level III Ecoregions. Regions that are between fuel-limited and climate-limited may have drivers of competing importance.

It is important to note that the daily area growth modeled in this research is an areal metric, rather than a linear metric. This areal unit is related to and slightly different from the linear unit of forward rate of spread. Understanding the drivers of linear rate of spread is also of importance, as fast fires can be very destructive and wildland fire management practices are strongly tied to linear units of progression. Work is underway to calculate the forward rate of spread for each daily fire perimeter in the FIRED dataset. Having that metric in hand will allow for the important drivers of the daily linear rate of spread across CONUS to be modeled and identified. Calculating the linear rate of spread, and dividing the complete dataset into smaller subregions will likely give specific insight into management practices for each subregion. Broadly, however, the results of this study show that at the daily scale, wildland fire growth is inhibited in complex landscapes.

## 4.5 Conclusion

The important features of random forest models were used to determine drivers of daily fire growth in the Level I ecoregions across CONUS. Physiographic heterogeneity is an important driver of daily wildland fire growth across CONUS. This indicates that daily wildland fire growth is inhibited in complex landscapes with a variety of surface features, rock and soil compositions, and vegetation patterns. The smaller Level I ecoregion spaces showed additional important drivers, suggesting that modeling the daily fire growth of smaller spaces will result in identifying drivers specific to each subregion.

## Chapter 5

### **FIRE Linear Forward Rate of Spread; How fast are our fastest fires?**

#### **5.1 Introduction**

Linear rate of forward fire spread (RoS) is an important fire behavior metric indicating when fires are most dangerous and difficult to control, meaning that our understanding and ability to forecast RoS is critical. Several factors contribute to creating dangerous wildfire conditions. A history of fire suppression and fuel accumulation have provided large, severe fires with abundant fuels [95]. The expansion of the WUI has broadened the fire niche by bringing ignition sources into environments not prone to fire in recent history with both high wind patterns and available fuel sources [108, 23]. This has facilitated the growth of larger human-caused fires [13, 38]. In 2018, a human-caused wildfire in Attica, Greece resulted in over 100 civilian fatalities [80]. The same year, the Camp Fire resulted in 85 fatalities, and destroyed the towns of Paradise and Concow, California [33]. In both cases extreme wind gusts, 30-34 m/s and 25 m/s for the Attica and Camp Fires respectively, interacted with complex terrain, causing rapid fire spread.

Our current understanding and ability to forecast RoS is founded on several decades of literature resulting from various wildfire experiments. Several studies have considered the relationships between terrain, weather and fuel as they pertain to fire behavior, and have been used to forecast the rate of spread (RoS) through empirical-based modeling [130]. The physical mechanisms of fire RoS have been examined in controlled environments either in small-scale laboratory experiments [119, 37, 18, 61, 19, 56] or in prescribed burns [48, 40, 94, 39]. These examinations of fire drivers and their interactions, along with our developed understanding of combustion through experimentation

have allowed us to investigate movement of the fire front through time. We have conceptualized the progression of wildfire as a perimeter, the outer edge of the fire that moves through space over time. Commonly, we describe this in context of the dominant wind direction, expecting the head or front of the fire to be the fastest section of the fire perimeter [140, 129]. The velocity of this section of the perimeter is typically called the *forward rate of spread*.

Here we will calculate the forward RoS metric for the FIRED daily burned area record. The daily area has been calculated for each fire event in the data set, and while comparing each consecutive day gives an indication of fire growth, it is not quite the same as RoS. Additionally, the relationship between the two (RoS and area increase) changes with time differently for each set of conditions. (Close to the ignition time of a fire, while it is still small, the heat flux is generally low and as such its RoS is slow. As the fire grows the combustion rate will increase, and the RoS will also increase. The fire will eventually reach a quasi-steady state of combustion for its set of conditions.) So while the measurements are related, one does not necessarily infer the other.

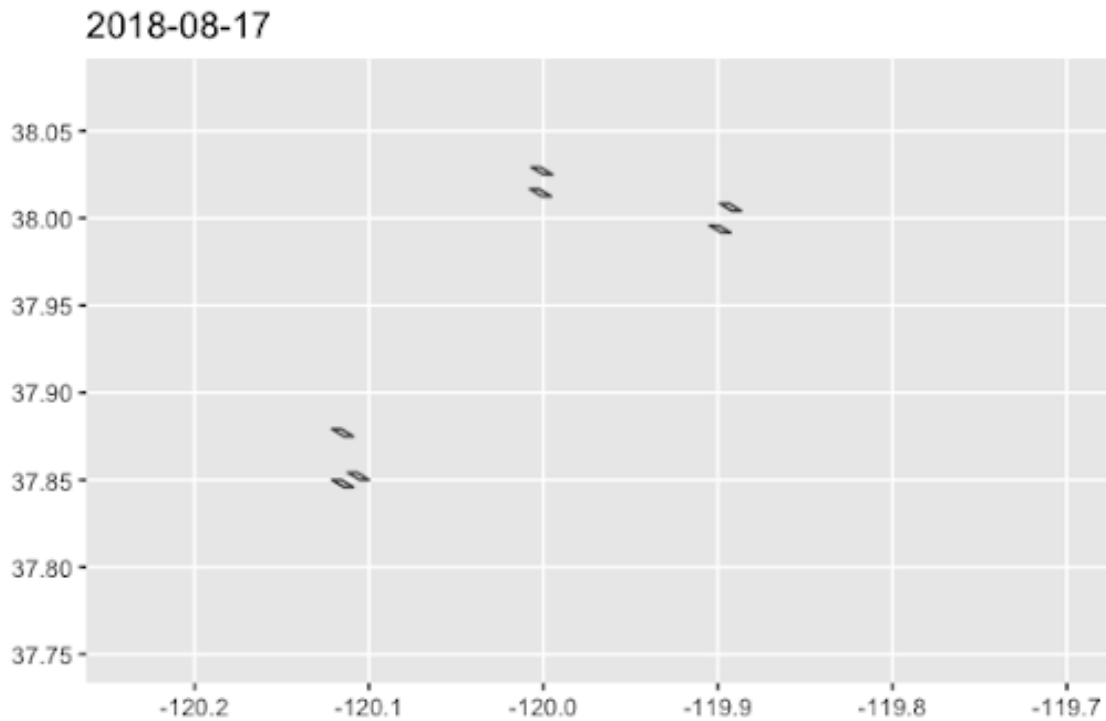
The RoS measurement will then be used to determine which were the fastest fires and where they were located in CONUS throughout the FIRED record (2001-2019). The goals of this research are to provide an accurate metric of RoS appropriate to the FIRED record, determine the upper 5% of fire speeds, and place the fastest fires in geographic context. The calculation of forward RoS across a twenty-year fire record at the daily growth level has not yet been accomplished, nor have the fastest fires and their locations been identified, making this research especially novel.

## 5.2 Methods

### 5.2.1 Bounding Fire Area and Calculating RoS Using Ellipses

This research is in its early stages of development. One challenge is that the data may show dispersion between points during the initial stages of an event, as shown in the first day of the FIRED record for the Rim Fire in Fig. 5.1.

Figure 5.1: Day 1 of the Rim Fire in California from the FIRED record.



However, the daily FIRED burned areas generally coalesce and show a clear direction of growth within a couple days (during the time that the heat flux is low, and the fire is still building toward a growth equilibrium). Again, the Rim Fire is given as an example in Fig. 5.2, Fig. 5.3, and Fig. 5.4.

Figure 5.2: Day 2 of the Rim Fire in California from the FIRED record.

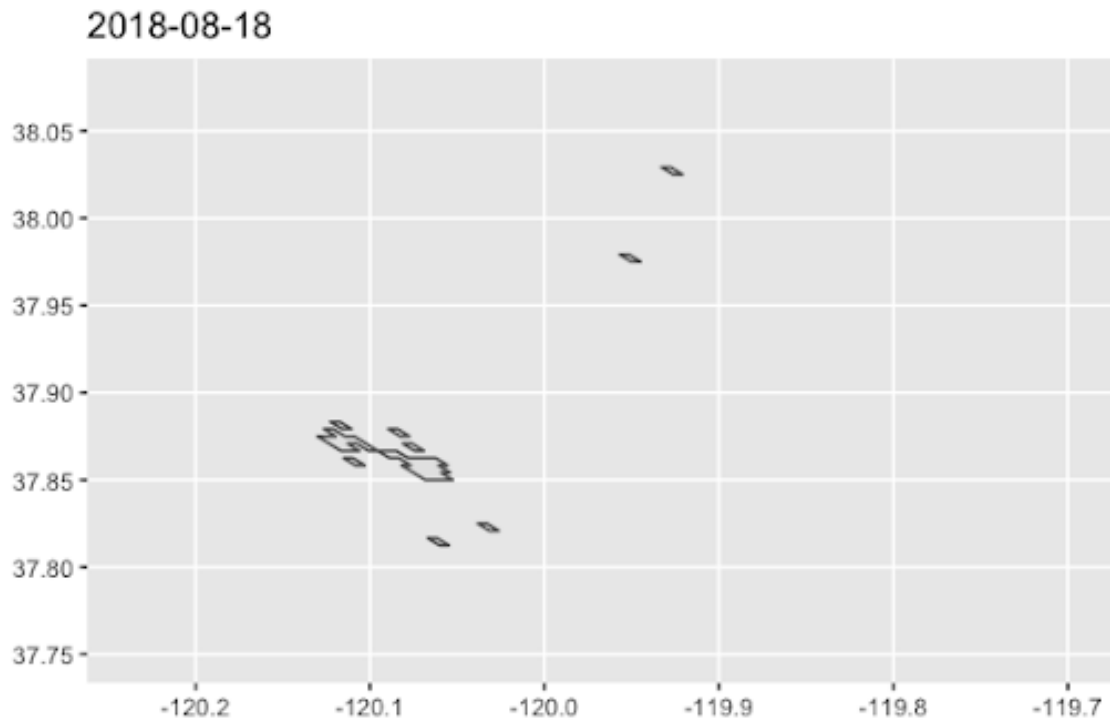


Figure 5.3: Day 3 of the Rim Fire in California from the FIRED record.

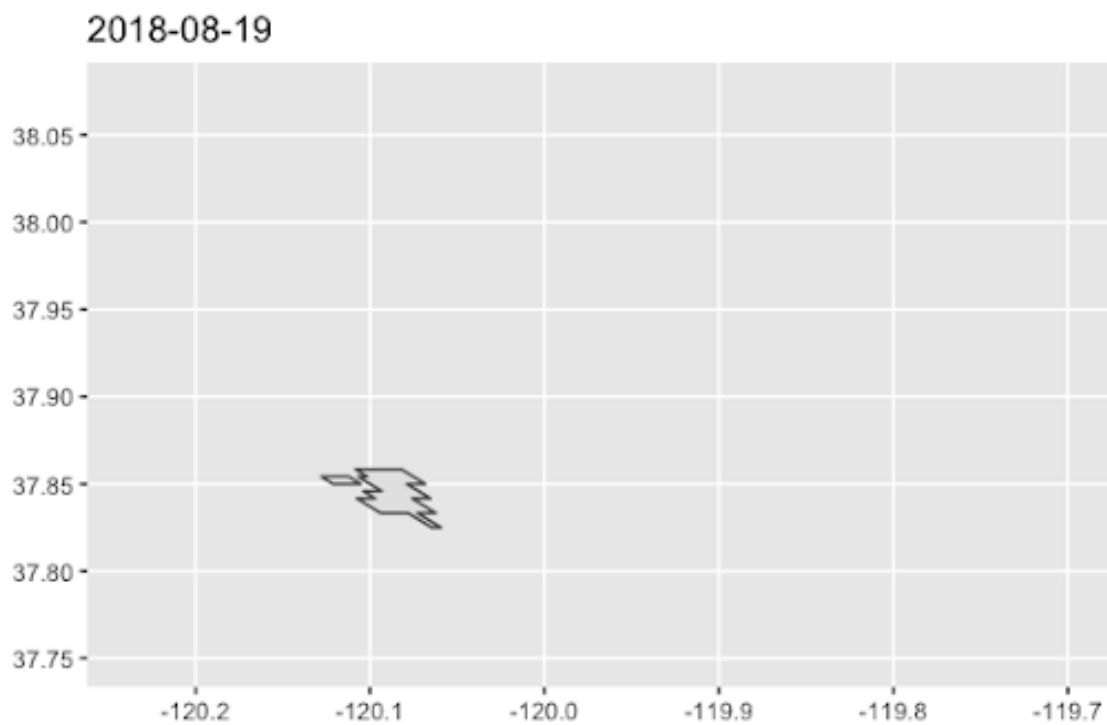
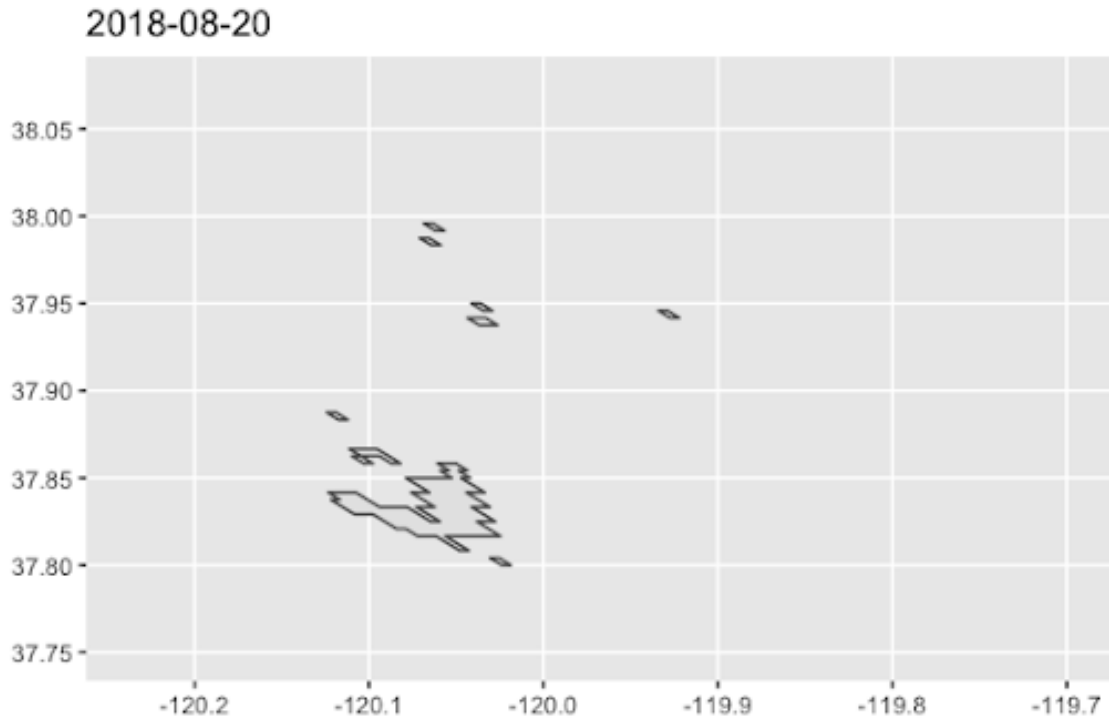


Figure 5.4: Day 4 of the Rim Fire in California from the FIRED record.

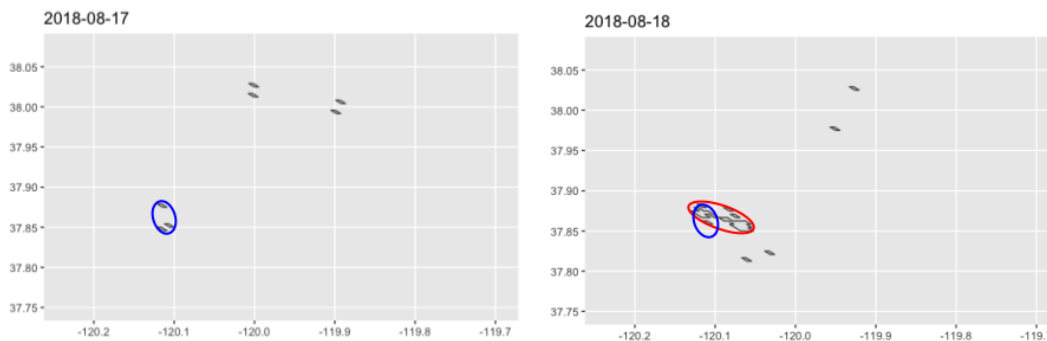


The approach to calculating forward RoS tested bounds consecutive days' burned area in ellipses, as shown in Fig. 5.5, as this shape has been found to adequately describe fire propagation [17, 16]. This idea is similar to the way a confidence ellipse is drawn over distributed data points, but is instead applied to the burned area pixels and their spatial locations [137].

This method removes any outliers, such as the pixels we see north of the main fire location in Fig. 5.1. These pixels are not part of the flaming front, and do not contribute to the forward RoS for this fire. This is identified by looking ahead at Day 2 (Fig. 5.2) and co-locating the first and second days' burned areas. Bounding the pixels using ellipses helps identify the forward front

in a way that aligns with how we conceptualize fire perimeters.

Figure 5.5: Bound the consecutive days' burned areas in ellipses as a first step in calculating the linear rate of spread.



After bounding subsequent days' pixels, we then draw a centerline through the second day's longest axis. The vector describing the daily forward RoS is the section of the centerline that intersects the first day's ellipse and the far edge of the second day's ellipse. This is shown in Figure 5.6 and Figure 5.7.

Figure 5.6: Draw a centerline through the second day's longest axis.

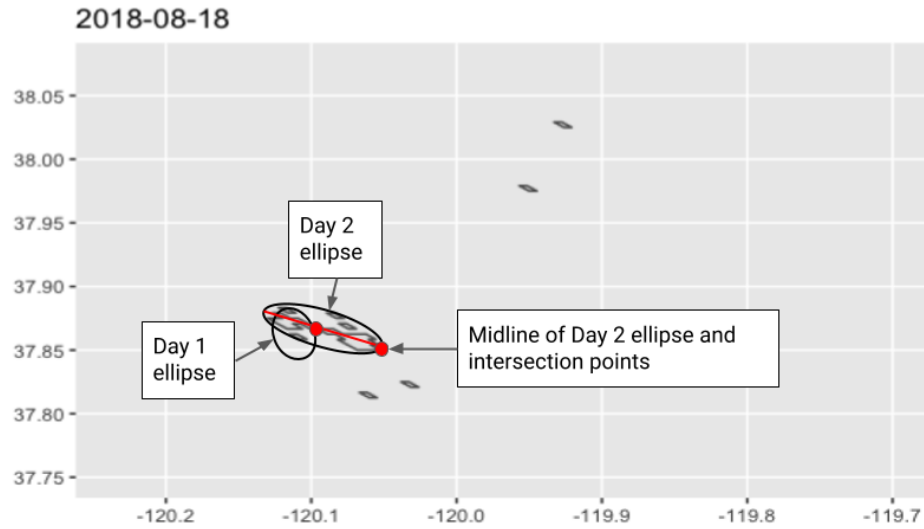
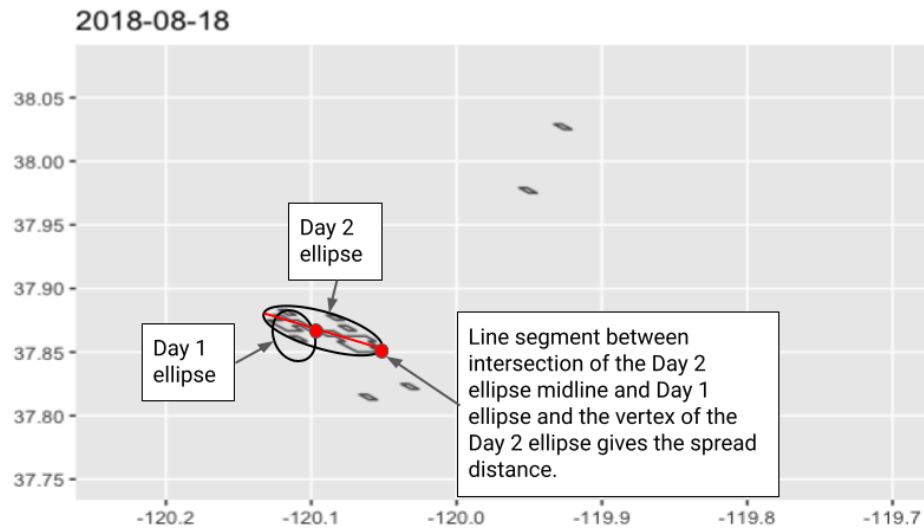


Figure 5.7: The vector describing the daily forward rate of spread is the section of the centerline that intersects the first day's ellipse and the farthest edge of the second day's ellipse.



A couple of concerns and limitations of this approach include sparse validation data and

computation accuracy. As a method of validation, it would be helpful to compare the resulting forward RoS calculations to those of comparable data sets. Unfortunately, there are not many data sets of daily burned area delineated by event (which is what makes FIRED so novel and valuable). The Global Fire Atlas (Andela et al., 2019) is a global record of fire size, duration, speed, and direction, which is to say, it includes a RoS metric. The RoS for each daily burned area in the Global Fire Atlas record is calculated by finding the most likely path between two burning points from two subsequent days by finding the shortest route between them. For clusters of pixels the assumption is made that the center point of the moment of the cluster is the origination point. This method results in the potential of several RoS metrics for a given day depending on how many individual pixels and clusters of pixels exist. This RoS measure does not represent the forward RoS because it does not focus on the flaming front of the fire. So, it is unclear how useful this metric is for validating the FIRED daily forward RoS. However, it is one of the only daily burn area fire records, so it would be useful to see if there is a general match in the RoS calculations, perhaps by comparing the FIRED RoS vector to the average direction and longest distance of the Global Fire Atlas RoS.

There is some concern of computation accuracy with the approach of bounding using ellipses. This method necessitates determining a spatial bounds for excluding the outlier pixels, and frequently the ellipse drawn around the main fire will not touch all sides. That is to say, the vertices may touch only two pixels. (Alternatively, an ellipsoid could be used, and the centerline drawn to divide the mass of the area in half the long way. This is not difficult to implement and compare with the ellipses, and will be explored.) However, it is helpful to remember that this calculation is for daily forward RoS, it is a generalization of a very dynamic measurement. As such, it should be sufficient to calculate the RoS in the way described.

Single day fires with only one pixel will be assigned a RoS of zero, as they will not have a subsequent day of growth. Fires with more than one day but only one pixel (at the same location) will also be assigned a value of zero as they have not moved through subsequent days.

### 5.2.2 Determining Fires of Unusual Size

To determine which are the fastest fires, we plan to examine the distribution of the RoS calculations. We will adopt the same approach as Tedim et al. (2018) [135] in their publication on extreme events, and examine the 90th, 95th, and 99th percentiles. We would expect that each region would have its own unique distribution of RoS, so it will be useful to divide the RoS calculations by the MODIS IGBP Land Cover classes and examine the percentiles for each region.

## **Chapter 6**

### **Conclusion**

#### **6.1 Introduction**

This chapter concludes the work contained in this dissertation by summarising the key research findings in relation to the research goals. A discussion of its societal and research contributions, as well as ongoing and future research opportunities follow.

#### **6.2 Overall Findings**

This research aimed to integrate remotely sensed data, wildland fire behavior modeling, and machine learning methods to further our understanding of the patterns and drivers of wildfire. High-resolution remotely-sensed datasets from several platforms were used to train random forest classification and regression models to identify drivers that matter at both the daily burned area and fire event scales, across individual case studies and collectively across thousands of events. WRF-Fire was used to investigate the intersection of drivers and how our current understanding of fire behavior, as represented by numeric models, compares to what we observe at sub-daily, daily, and event scales. The results indicate that environmental heterogeneity is important to fire spread in all regions across CONUS, at sub-daily and daily scales. Through this work we are better able to characterize fires that matter in terms of spread rate, which has implications within fire forecasting and future policy development.

## 6.3 Contributions

### 6.3.1 Fire Forecasting

Wildland fire behavior models have been used to further our understanding of fire behavior through experimentation and comparison with observational data [68], as well as for operational management where fire forecasts aid in determining suppression and evacuation strategies and the allocation of resources [103]. Uncertainty in model output can lead to a loss of faith and use of fire forecasts [111]. Persistent uncertainties still originate from input data sets, including fuel model assignment, and ignition location and timing data [26]. We currently lack data on the built environment, which is necessary for modeling and understanding fire spread through developed areas. These are the most critical spaces in terms of the danger presented to life and property, so it is imperative that data capturing the built environment are developed and integrated into fire forecasting and behavior research. Additionally, wildland fire behavior models are applied indiscriminately to simulate wildfires across CONUS, despite regional differences in fuel, terrain, and meteorology. We previously lacked the data necessary to investigate regional-scale drivers to inform the development of region-specific fire behavior models. This research contributes a method to resolve the gap in fine-scale, sub-seasonal fuel data, it contributes to our understanding of model limitations due to the lack in accurate ignition data, and it identifies regional-scale fire drivers. Wildland fire behavior models currently used in the U.S. were developed based on laboratory-scale experiments and prescribed burns, but are applied to scenarios spanning several days and thousands of acres. This work challenges the appropriateness of scaling fire mechanisms at the seconds and meters scale to the scale of days and kilometers. The drivers of fire in a laboratory setting are not necessarily the drivers of fire at a larger scale. At the very least, this work highlights the importance of integrating more physiographic diversity information into current behavior models to capture the effects of environmental heterogeneity on daily rate of spread. Models should be initiated using the best possible initiation data, including accurate ignitions and updated fuel layers.

### 6.3.2 Future Policy Development

In the U.S., the governance system that determines wildfire response is nested at local, state, and federal levels. While U.S. federal policy has acknowledged that wildfire has a critical ecological role to play, the practice of wildfire suppression has become normalized more than mitigation or acceptance [127], which has led in part to a more flammable landscape due to fuel accumulation. Additionally, indigenous and traditional fire management systems have been replaced by fuel management practices. These practices have played a role in increasing the number of fires [29], and have contributed to the risk of more severe wildfires [128, 92, 53]. Our understanding of and approach to fire is becoming increasingly important due to population increase and climate change. Current management strategies, which are focused mostly on basic resilience are not enough given the increasing WUI and climate conditions ripe for wildfire [90]. Little is known about the interactions between the atmosphere, terrain, and fuels in areas not historically prone to wildfire [36], which are essentially the spaces now exposed to ignition due to human activity. Future fuel and fire management policies are informed by our current understanding of fire behavior, as well as our anticipation of how that behavior will change under different conditions. The research presented here contributes to our understanding of fire behavior in different ecoregions across CONUS and it bolsters our ability to accurately model fire behavior. The work presented on regional-scale drivers may be used to inform policy development at a regional level. The method of updating fuel data for use within wildland fire behavior models may be used to forecast fire behavior under different fuel scenarios, which helps inform policy development with regard to fire and fuel management.

### 6.4 Future Work

Accurate ignition data is essential for modeling fire in heterogeneous fire domains. Future work that bounds the ignition location and time would greatly benefit modeling efforts, which in turn benefits our understanding of fire behavior. Identifying the drivers for the EPA Level II Ecoregions will further our understanding of fire behavior at a local level. Lastly, calculating the

forward rate of spread metric for the FIRED daily burned area record will distinguish between areal growth and the linear RoS commonly used in operational firefighting. The RoS measurement may be used to determine which were the fastest fires and where they were located in CONUS throughout the FIRED record (2001-2021). The calculation of forward RoS across a twenty-year fire record at the daily growth level has not yet been accomplished, nor have the fastest fires and their locations been identified, making this research especially novel.

## **6.5 Closing Summary**

To conclude, this research has contributed to our understanding of fire behavior through the integration of remotely sensed data, machine learning and wildland fire behavior modeling. Specifically this work shows that daily fire rate of spread is impeded in by environmental heterogeneity across CONUS; it presents a method for updating fuel data for use within wildland fire behavior models; and bounds the uncertainty associated with inaccurate ignition data within burned area and propagation direction forecasts. Collectively this research has improved our characterization of fires that matter as well as our ability to forecast fire behavior.

## Bibliography

- [1] Earth engine data catalog, sentinel-1. [https://developers.google.com/earth-engine/datasets/catalog/COPERNICUS\\_S1\\_GRD?hl=en](https://developers.google.com/earth-engine/datasets/catalog/COPERNICUS_S1_GRD?hl=en). Accessed: 2021-03-01.
- [2] Earth engine data catalog, sentinel-2. [https://developers.google.com/earth-engine/datasets/catalog/COPERNICUS\\_S2\\_SR](https://developers.google.com/earth-engine/datasets/catalog/COPERNICUS_S2_SR). Accessed: 2021-03-01.
- [3] Earth engine data catalog, usfs landscape change monitoring system v2020.5. [https://developers.google.com/earth-engine/datasets/catalog/USFS\\_GTAC\\_LCMS\\_v2020-5?hl=en](https://developers.google.com/earth-engine/datasets/catalog/USFS_GTAC_LCMS_v2020-5?hl=en). Accessed: 2021-03-01.
- [4] Environmental protection agency, climate change indicators: Wildfire. <https://www.epa.gov/climate-indicators/climate-change-indicators-wildfires>. Accessed: 2022-01-01.
- [5] Inciweb, east troublesome fire information. <https://inciweb.nwcg.gov/incident/7242/>. Accessed: 2021-06-01.
- [6] Integrated reporting of wildland-fire information. <https://nifc.maps.arcgis.com/apps>.
- [7] National interagency fire. <https://ftp.wildfire.gov>. Accessed: 2021-09-30.
- [8] Sentinel online, sentinel-1. <https://sentinels.copernicus.eu/web/sentinel/user-guides/sentinel-1-sar/applications/land-monitoring>. Accessed: 2022-01-01.
- [9] Sentinel online, sentinel-2. <https://sentinels.copernicus.eu/web/sentinel/user-guides/sentinel-2-msi/applications>. Accessed: 2022-01-01.
- [10] U.s. department of agriculture, biden-harris administration announces over \$1 billion in disaster relief funds for post-wildfire and hurricane recovery. <https://www.usda.gov/media/press-releases/2022/01/21/biden-harris-administration-announces-over-1-billion-disaster>. Accessed: 2022-01-01.
- [11] U.s. department of agriculture, forest health. <https://www.fs.fed.us/foresthealth/applied-sciences/mapping-reporting/detection-surveys.shtml>. Accessed: 2021-06-01.
- [12] John T Abatzoglou. Development of gridded surface meteorological data for ecological applications and modelling. *International Journal of Climatology*, 33(1):121–131, 2013.

- [13] John T Abatzoglou, Jennifer K Balch, Bethany A Bradley, and Crystal A Kolden. Human-related ignitions concurrent with high winds promote large wildfires across the usa. International journal of wildland fire, 27(6):377–386, 2018.
- [14] John T Abatzoglou and Crystal A Kolden. Climate change in western us deserts: potential for increased wildfire and invasive annual grasses. Rangeland Ecology & Management, 64(5):471–478, 2011.
- [15] Frank A Albin, James K Brown, Elizabeth D Reinhardt, and Roger D Ottmar. Calibration of a large fuel burnout model. International Journal of Wildland Fire, 5(3):173–192, 1995.
- [16] M. E. Alexander. Estimating the length-to-breadth ratio of elliptical forest fire patterns. Proceedings of the eighth conference on fire and forest meteorology, page Vol. 29., 1985.
- [17] Kerry Anderson, Gerhard Reuter, and Mike D Flannigan. Fire-growth modelling using meteorological data with random and systematic perturbations. International Journal of Wildland Fire, 16(2):174–182, 2007.
- [18] Wendy R Anderson, EA Catchpole, and BW Butler. Convective heat transfer in fire spread through fine fuel beds. International Journal of Wildland Fire, 19(3):284–298, 2010.
- [19] Wendy R Anderson, Miguel G Cruz, Paulo M Fernandes, Lachlan McCaw, Jose Antonio Vega, Ross A Bradstock, Liam Fogarty, Jim Gould, Greg McCarthy, Jon B Marsden-Smedley, et al. A generic, empirical-based model for predicting rate of fire spread in shrublands. International Journal of Wildland Fire, 24(4):443–460, 2015.
- [20] Stéfano Arellano-Pérez, Fernando Castedo-Dorado, Carlos Antonio López-Sánchez, Eduardo González-Ferreiro, Zhiqiang Yang, Ramón Alberto Díaz-Varela, Juan Gabriel Álvarez-González, José Antonio Vega, and Ana Daría Ruiz-González. Potential of sentinel-2a data to model surface and canopy fuel characteristics in relation to crown fire hazard. Remote Sensing, 10(10):1645, 2018.
- [21] MI Asensio-Sevilla, M Teresa Santos-Martín, David Álvarez-León, and L Ferragut-Canals. Global sensitivity analysis of fuel-type-dependent input variables of a simplified physical fire spread model. Mathematics and Computers in Simulation, 172:33–44, 2020.
- [22] Andreas Bachmann and Britta Allgöwer. Uncertainty propagation in wildland fire behaviour modelling. International Journal of Geographical Information Science, 16(2):115–127, 2002.
- [23] Jennifer K Balch, Bethany A Bradley, John T Abatzoglou, R Chelsea Nagy, Emily J Fusco, and Adam L Mahood. Human-started wildfires expand the fire niche across the united states. Proceedings of the National Academy of Sciences, 114(11):2946–2951, 2017.
- [24] Jennifer K Balch, Lise A St Denis, Adam L Mahood, Nathan P Mietkiewicz, Travis M Williams, Joe McGlinchy, and Maxwell C Cook. Fired (fire events delineation): An open, flexible algorithm and database of us fire events derived from the modis burned area product (2001–2019). Remote Sensing, 12(21):3498, 2020.
- [25] G. I. Baylor. Up, up and away. Proc. Roy. Soc., London A, 294:456–475, 1959.

- [26] Akli Benali, Ana CL Sá, Ana R Ervilha, Ricardo M Trigo, Paulo M Fernandes, and José MC Pereira. Fire spread predictions: Sweeping uncertainty under the rug. Science of the total environment, 592:187–196, 2017.
- [27] Stanley G Benjamin, Stephen S Weygandt, John M Brown, Ming Hu, Curtis R Alexander, Tatiana G Smirnova, Joseph B Olson, Eric P James, David C Dowell, Georg A Grell, et al. A north american hourly assimilation and model forecast cycle: The rapid refresh. Monthly Weather Review, 144(4):1669–1694, 2016.
- [28] António Bento-Gonçalves and António Vieira. Wildfires in the wildland-urban interface: Key concepts and evaluation methodologies. Science of the total environment, 707:135592, 2020.
- [29] David MJS Bowman, Crystal A Kolden, John T Abatzoglou, Fay H Johnston, Guido R van der Werf, and Mike Flannigan. Vegetation fires in the anthropocene. Nature Reviews Earth & Environment, 1(10):500–515, 2020.
- [30] David MJS Bowman, Grant J Williamson, John T Abatzoglou, Crystal A Kolden, Mark A Cochrane, and Alistair Smith. Human exposure and sensitivity to globally extreme wildfire events. Nature ecology & evolution, 1(3):1–6, 2017.
- [31] Paulo M Brando, Lucas Paolucci, Caroline C Ummenhofer, Elsa M Ordway, Henrik Hartmann, Megan E Cattau, Ludmila Rattis, Vincent Medjibe, Michael T Coe, and Jennifer Balch. Droughts, wildfires, and forest carbon cycling: A pantropical synthesis. Annual Review of Earth and Planetary Sciences, 47:555–581, 2019.
- [32] Leo Breiman. Random forests. Machine learning, 45(1):5–32, 2001.
- [33] Matthew J Brewer and Craig B Clements. The 2018 camp fire: Meteorological analysis using in situ observations and numerical simulations. Atmosphere, 11(1):47, 2019.
- [34] Marshall Burke, Anne Driscoll, Sam Heft-Neal, Jiani Xue, Jennifer Burney, and Michael Wara. The changing risk and burden of wildfire in the united states. Proceedings of the National Academy of Sciences, 118(2), 2021.
- [35] Natural Resources Canada. The state of canada’s forests (canadian forest service, ottawa), 2012. p. 72.
- [36] Adrián Cardil, Marcos Rodrigues, Joaquin Ramirez, Sergio de Miguel, Carlos A Silva, Michela Mariani, and Davide Ascoli. Coupled effects of climate teleconnections on drought, santa ana winds and wildfires in southern california. Science of The Total Environment, 765:142788, 2021.
- [37] WR Catchpole, EA Catchpole, BW Butler, RC Rothermel, GA Morris, and DJ Latham. Rate of spread of free-burning fires in woody fuels in a wind tunnel. Combustion Science and Technology, 131(1-6):1–37, 1998.
- [38] Megan E Cattau, Carol Wessman, Adam Mahood, and Jennifer K Balch. Anthropogenic and lightning-started fires are becoming larger and more frequent over a longer season length in the usa. Global Ecology and Biogeography, 29(4):668–681, 2020.

- [39] N Phillip Cheney, James S Gould, W Lachlan McCaw, and Wendy R Anderson. Predicting fire behaviour in dry eucalypt forest in southern australia. Forest Ecology and Management, 280:120–131, 2012.
- [40] NP Cheney, JS Gould, and Wr R Catchpole. Prediction of fire spread in grasslands. International Journal of Wildland Fire, 8(1):1–13, 1998.
- [41] RE Clark, AS Hope, S Tarantola, D Gatelli, Philip E Dennison, and Max A Moritz. Sensitivity analysis of a fire spread model in a chaparral landscape. Fire Ecology, 4(1):1–13, 2008.
- [42] Terry L Clark, Janice Coen, and Don Latham. Description of a coupled atmosphere–fire model. International Journal of Wildland Fire, 13(1):49–63, 2004.
- [43] Janice L Coen. Modeling wildland fires: A description of the coupled atmosphere-wildland fire environment model (cawfe). National Center for Atmospheric Research: Boulder, CO, USA, page 38, 2013.
- [44] Janice L Coen, Marques Cameron, John Michalakes, Edward G Patton, Philip J Riggan, and Kara M Yedinak. Wrf-fire: coupled weather–wildland fire modeling with the weather research and forecasting model. Journal of Applied Meteorology and Climatology, 52(1):16–38, 2013.
- [45] Janice L Coen, Marques Cameron, John Michalakes, Edward G Patton, Philip J Riggan, and Kara M Yedinak. Wrf-fire: coupled weather–wildland fire modeling with the weather research and forecasting model. Journal of Applied Meteorology and Climatology, 52(1):16–38, 2013.
- [46] Janice L Coen, E Natasha Stavros, and Josephine A Fites-Kaufman. Deconstructing the king megafire. Ecological applications, 28(6):1565–1580, 2018.
- [47] Tom W Coleman, Andrew D Graves, Zachary Heath, Robbie W Flowers, Ryan P Hanavan, Daniel R Cluck, and Daniel Ryerson. Accuracy of aerial detection surveys for mapping insect and disease disturbances in the united states. Forest ecology and management, 430:321–336, 2018.
- [48] W Wallace Covington and Stephen S Sackett. The effect of a prescribed burn in southwestern ponderosa pine on organic matter and nutrients in woody debris and forest floor. Forest Science, 30(1):183–192, 1984.
- [49] M. E. Crow. Aerodynamic sound emission as a singular perturbation problem. Stud. Appl. Math., 29:21–44, 1968.
- [50] Miguel G Cruz and Martin E Alexander. Uncertainty associated with model predictions of surface and crown fire rates of spread. Environmental Modelling & Software, 47:16–28, 2013.
- [51] Miguel G Cruz, Martin E Alexander, Andrew L Sullivan, James S Gould, and Musa Kilinc. Assessing improvements in models used to operationally predict wildland fire rate of spread. Environmental Modelling & Software, 105:54–63, 2018.
- [52] Philip E Dennison, Simon C Brewer, James D Arnold, and Max A Moritz. Large wildfire trends in the western united states, 1984–2011. Geophysical Research Letters, 41(8):2928–2933, 2014.

- [53] Daniel C Dey, Benjamin O Knapp, Mike A Battaglia, Robert L Deal, Justin L Hart, Kevin L O'Hara, Callie J Schweitzer, and Thomas M Schuler. Barriers to natural regeneration in temperate forests across the usa. New Forests, 50(1):11–40, 2019.
- [54] Julian D. Dole. Perturbation Methods in Applied Mathematics. Winsdell Publishing Company, 1967.
- [55] J. S. Fabnis, H. J. Giblet, and H. McDormand. Navier-stokes analysis of solid rocket motor internal flow. J. Prop. and Power, 2:157–164, 1980.
- [56] Mark A Finney, Jack D Cohen, Jason M Forthofer, Sara S McAllister, Michael J Gollner, Daniel J Gorham, Kozo Saito, Nelson K Akafuah, Brittany A Adam, and Justin D English. Role of buoyant flame dynamics in wildfire spread. Proceedings of the National Academy of Sciences, 112(32):9833–9838, 2015.
- [57] MD Flannigan, BM Wotton, GA Marshall, WJ De Groot, J Johnston, N Jurko, and AS Cantin. Fuel moisture sensitivity to temperature and precipitation: climate change implications. Climatic Change, 134(1):59–71, 2016.
- [58] William T Flatley, Charles W Lafon, and Henri D Grissino-Mayer. Climatic and topographic controls on patterns of fire in the southern and central appalachian mountains, usa. Landscape Ecology, 26(2):195–209, 2011.
- [59] William T Flatley, Charles W Lafon, Henri D Grissino-Mayer, and Lisa B LaForest. Changing fire regimes and old-growth forest succession along a topographic gradient in the great smoky mountains. Forest Ecology and Management, 350:96–106, 2015.
- [60] Jason M Forthofer, Bret W Butler, and Natalie S Wagenbrenner. A comparison of three approaches for simulating fine-scale surface winds in support of wildland fire management. part i. model formulation and comparison against measurements. International Journal of Wildland Fire, 23(7):969–981, 2014.
- [61] David Frankman, Brent W Webb, Bret W Butler, Daniel Jimenez, Jason M Forthofer, Paul Sopko, Kyle S Shannon, J Kevin Hiers, and Roger D Ottmar. Measurements of convective and radiative heating in wildland fires. International Journal of Wildland Fire, 22(2):157–167, 2012.
- [62] Dean Gesch, Michael Oimoen, Susan Greenlee, Charles Nelson, Michael Steuck, and Dean Tyler. The national elevation dataset. Photogrammetric engineering and remote sensing, 68(1):5–32, 2002.
- [63] Louis Giglio, Luigi Boschetti, David Roy, Anja A Hoffmann, Michael Humber, and Joanne V Hall. Collection 6 modis burned area product user's guide version 1.0. NASA EOSDIS Land Processes DAAC: Sioux Falls, SD, USA, 2016.
- [64] Anatoly A Gitelson, Galina P Keydan, and Mark N Merzlyak. Three-band model for noninvasive estimation of chlorophyll, carotenoids, and anthocyanin contents in higher plant leaves. Geophysical research letters, 33(11), 2006.
- [65] Noel Gorelick, Matt Hancher, Mike Dixon, Simon Ilyushchenko, David Thau, and Rebecca Moore. Google earth engine: Planetary-scale geospatial analysis for everyone. Remote sensing of Environment, 202:18–27, 2017.

- [66] F. Guillot and Z. Javalon. Acoustic boundary layers in propellant rocket motors. J. Prop. and Power, 5:331–339, 1989.
- [67] Evan Hjerpe, Yeon-Su Kim, and Leah Dunn. Forest density preferences of homebuyers in the wildland-urban interface. Forest Policy and Economics, 70:56–66, 2016.
- [68] Chad M Hoffman, Carolyn H Sieg, Rodman R Linn, William Mell, Russell A Parsons, Justin P Ziegler, and J Kevin Hiers. Advancing the science of wildland fire dynamics using process-based models. Fire, 1(2):32, 2018.
- [69] IBM. SPSS Statistics. download from vendor site, 2012. version 21.
- [70] Jose M Iniguez, Thomas W Swetnam, and Stephen R Yool. Topography affected landscape fire history patterns in southern arizona, usa. Forest Ecology and Management, 256(3):295–303, 2008.
- [71] Theresa B Jain, Andrew S Nelson, Benjamin C Bright, John C Byrne, and Andrew T Hudak. Biophysical settings that influenced plantation survival during the 2015 wildfires in northern rocky mountain moist mixed-conifer forests. Journal of Forestry, 120(1):22–36, 2022.
- [72] Pedro A Jiménez, Domingo Muñoz-Esparza, and Branko Kosović. A high resolution coupled fire–atmosphere forecasting system to minimize the impacts of wildland fires: Applications to the chimney tops ii wildland event. Atmosphere, 9(5):197, 2018.
- [73] Joshua M Johnston, Martin J Wooster, Ronan Paugam, Xianli Wang, Timothy J Lynham, and Lynn M Johnston. Direct estimation of byram’s fire intensity from infrared remote sensing imagery. International journal of wildland fire, 26(8):668–684, 2017.
- [74] W Matt Jolly, Mark A Cochrane, Patrick H Freeborn, Zachary A Holden, Timothy J Brown, Grant J Williamson, and David MJS Bowman. Climate-induced variations in global wildfire danger from 1979 to 2013. Nature communications, 6(1):1–11, 2015.
- [75] Van R Kane, C Alina Cansler, Nicholas A Povak, Jonathan T Kane, Robert J McGaughey, James A Lutz, Derek J Churchill, and Malcolm P North. Mixed severity fire effects within the rim fire: relative importance of local climate, fire weather, topography, and forest structure. Forest Ecology and Management, 358:62–79, 2015.
- [76] Robert E Keane, Robert Burgan, and Jan van Wagtendonk. Mapping wildland fuels for fire management across multiple scales: Integrating remote sensing, gis, and biophysical modeling. International Journal of Wildland Fire, 10(4):301–319, 2001.
- [77] Robert E Keane, Robert Burgan, and Jan van Wagtendonk. Mapping wildland fuels for fire management across multiple scales: Integrating remote sensing, gis, and biophysical modeling. International Journal of Wildland Fire, 10(4):301–319, 2001.
- [78] Crystal A Kolden and John Rogan. Mapping wildfire burn severity in the arctic tundra from downsampled modis data. Arctic, Antarctic, and Alpine Research, 45(1):64–76, 2013.
- [79] Kevin Krasnow, Tania Schoennagel, and Thomas T Veblen. Forest fuel mapping and evaluation of landfire fuel maps in boulder county, colorado, usa. Forest Ecology and Management, 257(7):1603–1612, 2009.

- [80] Kostas Lagouvardos, Vasiliki Kotroni, Theodore M Giannaros, and Stavros Dafis. Meteorological conditions conducive to the rapid spread of the deadly wildfire in eastern attica, greece. Bulletin of the American Meteorological Society, 100(11):2137–2145, 2019.
- [81] Henry Lao. Linear Acoustic Processes in Rocket Engines. PhD thesis, University of Colorado at Boulder, 1979.
- [82] Q. Lao, M. N. Cassoy, and K. Kirkpatrick. Acoustically generated vorticity from internal flow. J. Fluid Mechanics, 2:122–133, 1996.
- [83] Q. Lao, D. R. Kassoy, and K. Kirkkopru. Nonlinear acoustic processes in rocket engines. J. Fluid Mechanics, 3:245–261, 1997.
- [84] E Louise Loudermilk, J Kevin Hiers, and Joseph J O’Brien. The role of fuels for understanding fire behavior and fire effects. In Ecological restoration and management of longleaf pine forests, pages 107–122. CRC Press, 2017.
- [85] Jan Mandel. Fourier estimates for a multigrid. multigrid methods: theory, applications, and supercomputing, page 389, 2020.
- [86] Jan Mandel, Jonathan D Beezley, Lynn S Bennethum, Soham Chakraborty, Janice L Coen, Craig C Douglas, Jay Hatcher, Minjeong Kim, and Anthony Vodacek. A dynamic data driven wildland fire model. In International Conference on Computational Science, pages 1042–1049. Springer, 2007.
- [87] Jan Mandel, Jonathan D Beezley, and Adam K Kochanski. Coupled atmosphere-wildland fire modeling with wrf 3.3 and sfire 2011. Geoscientific Model Development, 4(3):591–610, 2011.
- [88] Samuel L Manzello, Kathleen Almand, Eric Guillaume, Stéphanie Vallerent, Stéphane Hameury, and Tuula Hakkarainen. Forum position paper the growing global wildland urban interface (wui) fire dilemma: Priority needs for research. Fire safety journal, 100, 2018.
- [89] Tyler C McCandless, Branko Kosovic, and William Petzke. Enhancing wildfire spread modelling by building a gridded fuel moisture content product with machine learning. Machine Learning: Science and Technology, 1(3):035010, 2020.
- [90] David B McWethy, Aníbal Pauchard, Rafael A García, Andrés Holz, Mauro E González, Thomas T Veblen, Julian Stahl, and Bryce Currey. Landscape drivers of recent fire activity (2001-2017) in south-central chile. PloS one, 13(8):e0201195, 2018.
- [91] Arjan JH Meddens, Jeffrey A Hicke, Lee A Vierling, and Andrew T Hudak. Evaluating methods to detect bark beetle-caused tree mortality using single-date and multi-date landsat imagery. Remote Sensing of Environment, 132:49–58, 2013.
- [92] Jessica Miesel, Alicia Reiner, Carol Ewell, Bernardo Maestrini, and Matthew Dickinson. Quantifying changes in total and pyrogenic carbon stocks across fire severity gradients using active wildfire incidents. Frontiers in Earth Science, 6:41, 2018.
- [93] CH Moeng, Jimy Dudhia, Joe Klemp, and Peter Sullivan. Examining two-way grid nesting for large eddy simulation of the pbl using the wrf model. Monthly weather review, 135(6):2295–2311, 2007.

- [94] Frédéric Morandini and Xavier Silvani. Experimental investigation of the physical mechanisms governing the spread of wildfires. International Journal of Wildland Fire, 19(5):570–582, 2010.
- [95] Max A Moritz, Tadashi J Moody, Meg A Krawchuk, Mimi Hughes, and Alex Hall. Spatial variation in extreme winds predicts large wildfire locations in chaparral ecosystems. Geophysical Research Letters, 37(4), 2010.
- [96] F. C. Mulick. Rotational axisymmetric mean flow and damping of acoustic waves in a solid propellant. AIAA J., 3:1062–1063, 1964.
- [97] F. C. Mulick. Stability of four-dimensional motions in a combustion chamber. Comb. Sci. Tech., 19:99–124, 1981.
- [98] Domingo Muñoz-Esparza, Branko Kosović, Pedro A Jiménez, and Janice L Coen. An accurate fire-spread algorithm in the weather research and forecasting model using the level-set method. Journal of Advances in Modeling Earth Systems, 10(4):908–926, 2018.
- [99] Muge Mutlu, Sorin C Popescu, and Kaiguang Zhao. Sensitivity analysis of fire behavior modeling with lidar-derived surface fuel maps. Forest Ecology and Management, 256(3):289–294, 2008.
- [100] Mikio Nakanishi and Hiroshi Niino. An improved mellor–yamada level-3 model with condensation physics: Its design and verification. Boundary-layer meteorology, 112(1):1–31, 2004.
- [101] JM Omernick. Aquatic ecoregions of the conterminous united states. Technical report, US Geological Survey, 1987.
- [102] James M Omernik and Glenn E Griffith. Ecoregions of the conterminous united states: evolution of a hierarchical spatial framework. Environmental management, 54(6):1249–1266, 2014.
- [103] Christopher D O’Connor, Matthew P Thompson, and Francisco Rodríguez y Silva. Getting ahead of the wildfire problem: Quantifying and mapping management challenges and opportunities. Geosciences, 6(3):35, 2016.
- [104] JMLM Palma, A Silva Lopes, VM Costa Gomes, C Veiga Rodrigues, Robert Menke, N Vasiljević, and Jakob Mann. Unravelling the wind flow over highly complex regions through computational modeling and two-dimensional lidar scanning. In Journal of Physics: Conference Series, volume 1222, page 012006. IOP Publishing, 2019.
- [105] SA Parks and JT Abatzoglou. Warmer and drier fire seasons contribute to increases in area burned at high severity in western us forests from 1985 to 2017. Geophysical Research Letters, 47(22):e2020GL089858, 2020.
- [106] Elsa Pastor, Luis Zárata, Eulalia Planas, and Josep Arnaldos. Mathematical models and calculation systems for the study of wildland fire behaviour. Progress in Energy and Combustion Science, 29(2):139–153, 2003.
- [107] Fabian Pedregosa, Gaël Varoquaux, Alexandre Gramfort, Vincent Michel, Bertrand Thirion, Olivier Grisel, Mathieu Blondel, Peter Prettenhofer, Ron Weiss, Vincent Dubourg, et al. Scikit-learn: Machine learning in python. the Journal of machine Learning research, 12:2825–2830, 2011.

- [108] Volker C Radeloff, David P Helmers, H Anu Kramer, Miranda H Mockrin, Patricia M Alexandre, Avi Bar-Massada, Van Butsic, Todd J Hawbaker, Sebastián Martinuzzi, Alexandra D Syphard, et al. Rapid growth of the us wildland-urban interface raises wildfire risk. Proceedings of the National Academy of Sciences, 115(13):3314–3319, 2018.
- [109] Raj K Rai, Larry K Berg, Branko Kosović, Jeffrey D Mirocha, Mikhail S Pekour, and William J Shaw. Comparison of measured and numerically simulated turbulence statistics in a convective boundary layer over complex terrain. Boundary-Layer Meteorology, 163(1):69–89, 2017.
- [110] Krishna Rao, A Park Williams, Jacqueline Fortin Flefil, and Alexandra G Konings. Sar-enhanced mapping of live fuel moisture content. Remote Sensing of Environment, 245:111797, 2020.
- [111] Claire Rapp, Emily Rabung, Robyn Wilson, and Eric Toman. Wildfire decision support tools: An exploratory study of use in the united states. International journal of wildland fire, 29(7):581–594, 2020.
- [112] R. S. Richards and A. M. Brown. Coupling between acoustic velocity oscillations and solid propellant combustion. J. Prop. and Power, 5:828–837, 1982.
- [113] Brendan M Rogers, Jennifer K Balch, Scott J Goetz, Caroline ER Lehmann, and Merritt Turetsky. Focus on changing fire regimes: interactions with climate, ecosystems, and society. Environmental Research Letters, 15(3):030201, 2020.
- [114] Matthew G Rollins. Landfire: a nationally consistent vegetation, wildland fire, and fuel assessment. International Journal of Wildland Fire, 18(3):235–249, 2009.
- [115] Matthew G Rollins. Landfire: a nationally consistent vegetation, wildland fire, and fuel assessment. International Journal of Wildland Fire, 18(3):235–249, 2009.
- [116] Richard C Rothermel. A mathematical model for predicting fire spread in wildland fuels, volume 115. Intermountain Forest & Range Experiment Station, Forest Service, US . . . , 1972.
- [117] Richard C Rothermel. How to predict the spread and intensity of forest and range fires, volume 143. US Department of Agriculture, Forest Service, Intermountain Forest and Range . . . , 1983.
- [118] Richard C Rothermel and Hal E Anderson. Fire spread characteristics determined in the laboratory, volume 30. Intermountain Forest & Range Experiment Station, Forest Service, US . . . , 1966.
- [119] Richard C Rothermel and Hal E Anderson. Fire spread characteristics determined in the laboratory, volume 30. Intermountain Forest & Range Experiment Station, Forest Service, US . . . , 1966.
- [120] David P Roy, Junchang Ju, Kristi Kline, Pasquale L Scaramuzza, Valeriy Kovalskyy, Matthew Hansen, Thomas R Loveland, Eric Vermote, and Chunsun Zhang. Web-enabled landsat data (weld): Landsat etm+ composited mosaics of the conterminous united states. Remote Sensing of Environment, 114(1):35–49, 2010.

- [121] Kevin C Ryan and Tonja S Opperman. Landfire—a national vegetation/fuels data base for use in fuels treatment, restoration, and suppression planning. Forest Ecology and Management, 294:208–216, 2013.
- [122] Joe H Scott. Standard fire behavior fuel models: a comprehensive set for use with Rothermel’s surface fire spread model. US Department of Agriculture, Forest Service, Rocky Mountain Research Station, 2005.
- [123] Joe H Scott and Robert E Burgan. A comprehensive set of standard fire behavior fuel models for use with rothermel’s surface fire spread model. Gen. Tech. Rep. RMRS-GTR-153. Fort Collins, CO: US Department of Agriculture, Forest Service, Rocky Mountain Research Station.
- [124] William C Skamarock, Joseph B Klemp, Jimy Dudhia, David O Gill, Dale M Barker, Wei Wang, and Jordan G Powers. A description of the advanced research wrf version 2. Technical report, National Center For Atmospheric Research Boulder Co Mesoscale and Microscale . . . , 2005.
- [125] T. M. Smitty, R. L. Coach, and F. B. Höndra. Unsteady flow in simulated solid rocket motors. In 16st Aerospace Sciences Meeting, number 0112 in 78. AIAA, 1978.
- [126] Michael C Stambaugh and Richard P Guyette. Predicting spatio-temporal variability in fire return intervals using a topographic roughness index. Forest Ecology and Management, 254(3):463–473, 2008.
- [127] Toddi A Steelman and Caitlin A Burke. Is wildfire policy in the united states sustainable? Journal of forestry, 105(2):67–72, 2007.
- [128] Barbara A Strom and Peter Z Fulé. Pre-wildfire fuel treatments affect long-term ponderosa pine forest dynamics. International Journal of Wildland Fire, 16(1):128–138, 2007.
- [129] AL Sullivan and JS Gould. Wildland fire rate of spread. Encyclopedia of Wildfires and Wildland-Urban Interface (WUI) Fires, pages 1–4, 2018.
- [130] Andrew L Sullivan. Wildland surface fire spread modelling, 1990–2007. 2: Empirical and quasi-empirical models. International Journal of Wildland Fire, 18(4):369–386, 2009.
- [131] Andrew L Sullivan and Stuart Matthews. Determining landscape fine fuel moisture content of the kilmore east ‘black saturday’ wildfire using spatially-extended point-based models. Environmental Modelling & Software, 40:98–108, 2013.
- [132] Ritu Taneja, James Hilton, Luke Wallace, Karin Reinke, and Simon Jones. Effect of fuel spatial resolution on predictive wildfire models. International journal of wildland fire, 30(10):776–789, 2021.
- [133] Joseph D. Taum. Investigation of flow turning phenomenon. In 20th Aerospace Sciences Meeting, number 0297 in 82. AIAA, 1982.
- [134] Alan H Taylor and Carl N Skinner. Spatial patterns and controls on historical fire regimes and forest structure in the klamath mountains. Ecological Applications, 13(3):704–719, 2003.

- [135] Leone V. Amraoui M. Bouillon C. Coughlan M.R. Delogu G.M. Fernandes P.M. Ferreira C. McCaffrey S. McGee T.K. Tedim, F. and J. Parente. Defining extreme wildfire events: difficulties, challenges, and impacts. Fire, page 1(1) p.9, 2018.
- [136] David M Theobald, Dylan Harrison-Atlas, William B Monahan, and Christine M Albano. Ecologically-relevant maps of landforms and physiographic diversity for climate adaptation planning. PloS one, 10(12):e0143619, 2015.
- [137] Wenzhong S. Wang, B. and M. Zelang. Confidence analysis of standard deviational ellipse and its extension into higher dimensional euclidean space. PloS one, page 10.3, 2015: e0118537.
- [138] Paul A Werth, Brian E Potter, Martin E Alexander, Craig B Clements, Miguel G Cruz, Mark A Finney, Jason M Forthofer, Scott L Goodrick, Chad Hoffman, W Matt Jolly, et al. Synthesis of knowledge of extreme fire behavior: volume 2 for fire behavior specialists, researchers, and meteorologists. Gen. Tech. Rep. PNW-GTR-891. Portland, OR: US Department of Agriculture, Forest Service, Pacific Northwest Research Station. 258 p., 891, 2016.
- [139] Anthony L Westerling, Hugo G Hidalgo, Daniel R Cayan, and Thomas W Swetnam. Warming and earlier spring increase western us forest wildfire activity. science, 313(5789):940–943, 2006.
- [140] BM Wotton, RS McAlpine, and MW Hobbs. The effect of fire front width on surface fire behaviour. International Journal of Wildland Fire, 9(4):247–253, 1999.
- [141] Robert A. Zeddini. Injection-induced flows in porous-walled ducts. AIAA Journal, 14:766–773, 1981.